Hardware-in-Loop Simulation of Battery Storage Systems for Power System Applications

by

Damon Bazargan

A thesis submitted to the Faculty of Graduate Studies of

The University of Manitoba

in partial fulfillment of the requirements for the degree of

Master of Science

Department of Electrical and Computer Engineering

University of Manitoba

Winnipeg, Manitoba, Canada

ABSTRACT

Batteries are important energy storage devices and are used in different applications. The purpose of this thesis is to study behavior and characteristics of batteries when used in system-level design process. In addition, the use of hardware-in-loop (HIL) simulation of batteries for power system applications is studied. The thesis also aims to investigate the ability of HIL in alleviating the need for extensive and detailed modeling of battery storage systems and to improve the accuracy of the simulation of systems where they are used. The major problem of using battery models is that they are greatly affected by external factors such as temperature and history of the charge/discharge regimes. An HIL scheme eliminates the need for mathematical modeling of batteries by interfacing them directly to the simulator, where charging and discharging regimes, state of charge estimation methods and efficiency can be investigated.

Acknowledgment

First and foremost, I would like to thank my academic advisor, Prof. Shaahin Filizadeh, for his direction, support and encouragement during my M.Sc. studies. I extend my gratitude to Manitoba Hydro International and MITACS internship program for their financial support. I would like to appreciate Manitoba HVDC Research Centre staff especially Randy Wachal and Danny Northcott who shared generously their experience and knowledge with me. I would like to thank my parents, Maedeh and Reza for their love and support over these many years. Finally, I would also like to express my appreciation for my close friend Garry Bistyak for his help and support.

List of Acronyms

BESS: Battery Energy Storage System

BMS: Battery Management System

CAN: Controller Area Network

CCCV: Constant Current Constant Voltage

DoD: Depth of Discharge

EIS: Electrochemical Impedance Spectroscopy

HEV: Hybrid Electric Vehicle

HIL: Hardware in Loop

OCV: Open Circuit Voltage

PLL: Phase Lock Loop

SoC: State of Charge

SoH: State-of-Health

STATCOM: Static Synchronous Compensator

VSC: Voltage Source Converter

TABLE OF CONTENTS

1. Introduction 1
1.1 Problem Definition 4
1.2 Research Methodology 5
1.3 Thesis Organization 9

2. Battery Energy Storage 11
2.1 Battery Characteristics and Specifications 16
2.1.1 State of Charge (SoC) and State of Health (SoH) 22
2.1.2 Efficiency 26
2.2 Battery Models 28
2.2.1 Thevenin Model 29
2.2.2 Randle's Model 31
2.2.3 Shepherd Model 35
2.3 BES in Power Systems 42

3. BESS in Wind Farms 44
3.1 Wind Power 44
3.2 Configuration of Type 1 Wind Farm 49
3.2.1 BESS Sizing 50
3.3 DC-DC Converter 52
3.4 Voltage Source Converter (VSC) 57

4. Experiments 65
4.1 Description of a Type 1 Wind Farm 66
4.1.1 PSCAD Simulation Results 70
4.2 HIL Setup 75
4.2.1 HIL Simulation Results 78
4.2.2 Using HIL for Efficiency Measurement 85

5. Conclusions, Contributions and Future Directions 87
5.1 Contributions 87
5.2 Recommendations for Future Work 90

References 92

LIST OF FIGURES

1.1 Schematic of Hardware In the Loop Simulation. 6
1.2 Schematic of Hardware In the Loop Simulation with an actuator. . 8
1.3 Schematic of Reduced-Scale Hardware In the Loop Simulation. . . . 9

2.1 A sample battery pack with multiple series batteries and fuse and contactors 14
2.2 Shows passive cell balancing on right and active cell balancing on the left 16
2.3 Discharge curve of LPF26650P Lithium-Ion battery 17
2.4 Charge curve of LPF26650P Lithium-Ion battery. 18
2.5 Discharge curve of LPF26650P Lithium-Ion battery Versus capacity. 20
2.6 Comparison of energy density in different battery types [1]. 21
2.7 Comparison of specific energy in different battery types [1]. 21
2.8 Rested and Unrested OCV of PC625 Odyssey Lead-acid battery Versus SoC. Presented equation shows linear relation between OCV and SoC. 24
2.9 Rested OCV of PC625 Odyssey Lead-acid battery with different rest time Versus SoC. 25
2.10 Method to calculate efficiency. 28
2.11 Thevenin or ideal battery model. 30
2.12 Internal resistance vs state of charge. 31
2.13 An experiment to measure internal resistance of battery. 32
2.14 Randle's model. 33
2.15 An experiment to measure Randle model's parameters. 34
2.16 Actual and Shepherd model discharge curve for PC625 Odyssey lead-acid battery. 37
2.17 Actual and Shepherd model discharge curve for LPF26650P K2 energy lithium ion battery. 38
2.18 Comparison of Shepherd model and a real battery in pulsed charging process. 39
2.19 Comparison of Thevenin model and a real battery in pulsed charging process. 40
2.20 Comparison of Randle model and a real battery in pulsed charging process. 41

3.1 Effect of change of wind speed in wind power, figure on the top shows wind speed vs time, the one at the middle shows wind power VS time and the last figure shows angle of pitch vs time. 47
3.2 Schematic of a typical type 1 wind farm. 50
3.3 STATCOM with hybrid battery energy storage. 51
3.4 Sample power variation of wind. 52
3.5 A Bidirectional converter. 54
3.6 Duty cycle generation. 55
3.7 Control block diagram of DC-DC converter. 55
3.8 Battery model connected to DC-DC converter 56
3.9 A single phase VSC. 58
3.10 Output waveform of a single phase VSC. 58
3.11 PWM technique. 59
3.12 Schematic of VSC connection to grid. 60
3.13 DQ Control diagram of a VSC. 63
3.14 VSC simulation results. 63

4.1 Schematic diagram of simulated case study. 67
4.2 Schematic diagram of case study. 68
4.3 Control schematic of case study. 69
4.4 Wind speed variations. 71
4.5 Pitch angle variations. 71
4.6 Produced wind power, exported power from wind farm and contribution of BESS 72
4.7 Battery current profile. 72
4.8 DC link voltage. 73
4.9 Produced wind power, exported power from wind farm and contribution of BESS. 74
4.10 Battery current profile. 74
4.11 Produced wind power, exported power from wind farm and contribution of BESS. 75
4.12 Battery current profile. 76
4.13 HIL schematic. 76
4.14 Hall effect sensor used. 78
4.15 Runtime environment in RSCAD. 79
4.16 Produced active power of wind turbine. 80
4.17 Exported active power to grid. 80
4.18 BESS power profile. 81
4.19 DC link voltage. 82
4.20 Battery current profile. 82
4.21 Battery voltage profile. 83
4.22 Battery SoC. 83

4.23 Battery current change with a typical wind gust. 84

1. INTRODUCTION

Batteries are used in a wide spectrum of applications and power levels ranging from fraction of a watt to megawatts [1, 2]. Batteries are either a primary source of energy, or are used with another source of energy, for example with a diesel or interenal combustion engine in a hybrid vehicle. They can also be used as backup power supply, which means they rarely provide energy, e.g. back up energy storage in power systems. Their application can be mobile, such as in a cell phone, or stationary such as in a wind farm to level the generated power.

A battery is a device that supplies electrical power through chemical reactions and is found in a variety of chemistries such as lead acid, nickel-metal hydride or lithium ion. Regardless the specific chemistry used in a battery or its application, in system-level design it is important to understand how to use them properly. Batteries should be protected against factors like low state-of-charge (SoC), over-current and over-temperature. Usually battery management systems (BMS) are used to protect batteries. It is necessary to have an understanding of the capacity and ratings of a battery and how it reacts and how its characteristics degrades over time. Battery energy storage systems (BESS) are composed of many battery

packs each of which composed of battery cells. They have many applications in power systems, which will be discussed in detail in next chapters.

The scope of this thesis is to study important parameters of a battery with which a system level design can be done. In particular the research aims to develop a hardware-in-loop simulation setup to investigate how a real battery acts in a power system case study in comparison to battery models and to measure its efficiency. A type 1 wind farm has been chosen as the case study. In a type 1 wind farm, induction generators are used and are connected to the grid. In this type of wind farm capacitor banks are used to provide the required reactive power for induction generators [3, 4] . This type of wind farm is commonly used. Other types of wind farms are discussed in [5]. Generally the speed of wind should be considered as a non-deterministic factor in a wind farm. In most studies a probability function is used to describe the behavior of wind speed. Weibull and Raylieh probability distribution functions are commonly used in this context [6]. As speed of wind changes the produced power in a wind farm changes. These power variations are mainly caused by the effects of turbulence, wind shear and tower shadow and control system in a power system [3].

BESS are used in order to level the produced active power in a wind farm. Depending on the type of the generator or the structure of the wind farm, BESS might be connected to a DC-DC converter and/or to a voltage source converter (VSC). DC-DC converters are usually used to increase the voltage level of the

battery packs and VSCs are used to connect batteries to an AC power source. In recent studies BESS are connected to static synchronous compensator (STATCOM) devices to level active and reactive power at the same time [7,8]. STATCOM increases power quality of the grid:(voltage variation is directly related to active and reactive power variations); by controlling the exported active and reactive power from the wind farm voltage variations decrease [7]. A common STATCOM consists of a voltage source converter and a DC source, which is a DC capacitor. A STATCOM is not able to provide continues active power compensation unless a battery energy storage (BES) is connected in parallel to its DC capacitor [8].

The use of a battery in this case study is to level energy generation in the wind farm. For example when the wind speed is low the power produced will be less and the BES should provide the rest of the energy and when the wind speed is high, the wind power generated will be high and the extra energy should charge the BES. Different charging strategies can be chosen for batteries, e.g. constant current-constant voltage (CCCV) or pulsed charging. In most BESS applications, in which charging time is uncertain the CCCV method is used. It provide possibility of maximum energy harvesting during charging time. The uncertainty of renewable energy sources is a major drawback of wind power generation technology especially for isolated power systems. Using BESS in renewable energy systems will lead to higher customer satisfaction and social acceptability of renewable based technology.

A type 1 wind farm will be implemented in the PSCAD/EMTDC simulation

environment and then in the RSCAD environment for real-time simulation. This implementation includes required power electronics, which are needed for connecting BESS to the grid. Appropriate controllers are designed to control the system. To compare a real battery with models, a Shepherd model and a Thevenin model of batteries will be developed for lead-acid and lithiom-ion chemistries.

1.1 Problem Definition

Battery characteristics change by time because of various chemical reactions that happen inside them. This phenomenon is called aging, which becomes more severe as the battery undergoes more of its charge/discharge cycles. It starts gradually and depending on temperature, discharge rate and depth of discharge (DoD) in the cycles, might happen before or after 3000 cycles. Some research have been done to investigate how aging happens and how to model it [9–11]. In [12] the proposed model tries to adapt its parameters according to aging to remain accurate although validation of these models are not always possible. In some studies accelerated aging is considered to validate test results. In [13] high temperature is used to facilitate accelerated aging condition. Aging will affect cell voltage. It increases cell internal resistance and decreases cell capacity. These changes will make models less accurate especially if the duration of simulation is long.

Change of characteristics of batteries is also a problem at the time of sizing battery energy storage (BES) for a system. Over time the capacity and the efficiency

of battery cells decrease. This might prevent the BES to provide the system with the required energy. On the other hand over-sizing the BES increases the capital cost of the system. Therefore while using battery models one should consider the fact that in real implementation some battery characteristics will change, which are not considered in the models.

In addition, used batteries are difficult to model. Used batteries might be utilized in applications other than their orginal one; e.g. a hybrid electric vehicle (HEV) battery pack might no longer be appropriate to be used in a vehicle as it has lost its capacity and efficiency but is still good to be used in a stationary application in power systems; For example as a backup energy supplier or in a wind farm to level the generated energy.

As battery characteristics change by time, simulation results would be different from the real case. In addition, efficiency of a battery is not considered in most of battery models.

1.2 Research Methodology

To solve the problem of inaccuracy of battery models it is suggested to use hardware-in-loop (HIL) as the closest alternative to real field experience. HIL simulation has been used for controller assessment for many years especially in vehicle, aerospace and power industries. This methodology provides exhaustive testing opportunity and prevents costly and damaging failures. It can enable more tests to be per-

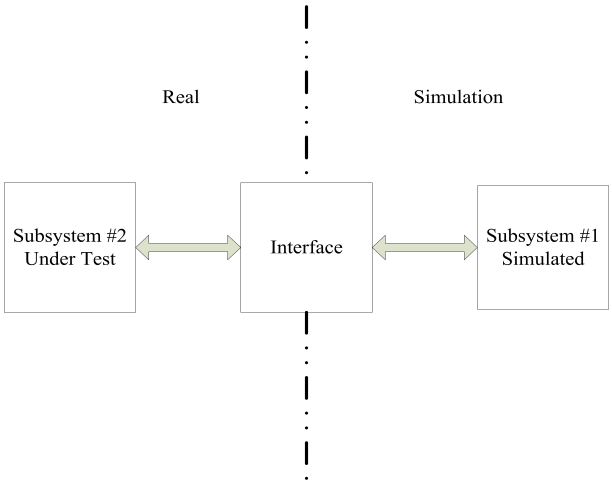

Fig. 1.1: Schematic of Hardware In the Loop Simulation.

formed than on real systems.

In HIL simulation one part of the closed loop simulation is replaced by a real device, which is the subsystem under test. The HIL simulation consists of a device under test, a real-time simulator and an interface. This will provide the opportunity for testing the device under field conditions. This real part should communicate with the simulation through an interface. For this purpose, sampling time should be chosen small enough to take into account the smallest time constant of the tested subsystem. In Fig. 1.1 a schematic diagram of an HIL Simulation is shown. Subsystem 2 has physical existence and is under test. The interface module is used to provide communication for the two subsystems.

This type of simulation stands in between software simulation and hardware prototyping of a system. Software simulation is certainly less expensive but the accuracy of simulation depends on the accuracy of the used models. In models,

some parameters might be non stationary and vary with time. Thus model uncertainty is difficult to take into account. Moreover undesirable factors such as electromagnetic disturbances are difficult to be considered in software simulations. On the other hand results from a hardware prototype are more reliable, but it is more expensive to develop. In some cases it might be impossible to do various types of tests on a prototype system, for example in systems including a hydrogen reservoir, as it is explosive. Software simulation is a preliminary step before implementing HIL simulation to define and tune control algorithm. HIL simulation is used for validation of tests of the real time system before implementation of the actual process.

HIL simulation is currently being used in many fields, e.g. vehicle component evaluation, robotics, power electronics and automation systems [14–16]. In some cases there is a need for an emulation device to impose same condition as the tested subsystem should be experiencing in the field. In Fig. 1.2 a schematic diagram of an HIL simulation with an actuator is shown. As it is shown, in addition to the subsystem under test, an actuator controller is communicating with the interface. The actuator device emulates effect of simulation on the subsystem being tested. The interface is used to transmit information from/to actuator and subsystem2.

The power rating of the emulation device should be greater than power rating of the subsystem under test. Recently in development of HIL simulation for high power applications, reduced-scale power systems are used to validate results at

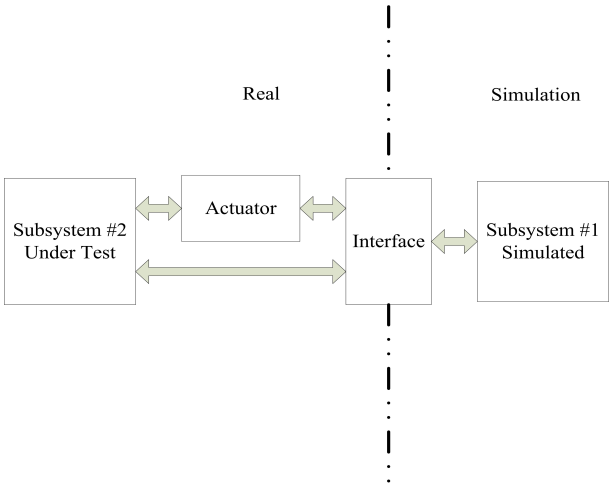

Fig. 1.2: Schematic of Hardware In the Loop Simulation with an actuator.

first. In this case the tested part will be replaced by an equivalent subsystem with reduced power ratings. In [17,18] a reduced scale HIL has been developed and real batteries have been used. In order to compensate for this replacement a power adaptation block is required. This power adaptation block involves a linear power amplification. This block amplifies effect of reduced-scaled subsystem, which is under test [19].

In Fig. 1.3 a schematic diagram of a reduced-scale HIL simulation is shown. The power amplifier scales down/up the emulated effect of simulation on the subsystem being tested. The interface is used to transmit information from/to actuator and subsystem 2. In order to alleviate differences between the power rating of subsystems it is also suggested to use per-unit values instead of absolute values [17]. In this case all of the power rating will be considered as per-unit.

In this thesis to study a battery energy storage system in a type 1 wind farm, a

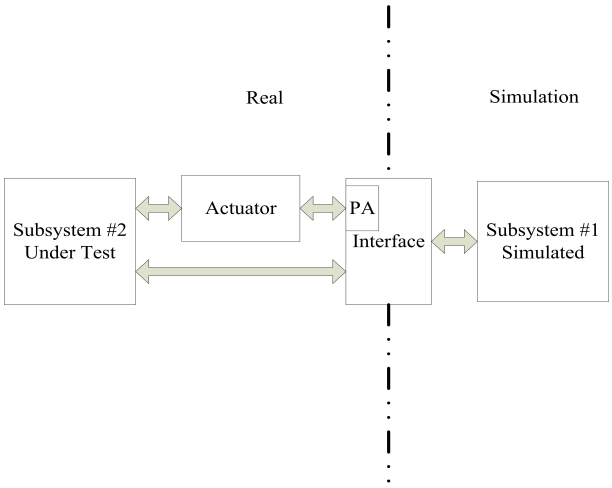

Fig. 1.3: Schematic of Reduced-Scale Hardware In the Loop Simulation.

reduced-scale HIL simulation setup is used. Real-Time Digital Simulator(RTDS) is used as real-time simulation environment. It is composed of specially designed hardware and software. RTDS hardware includes digital signal processors and advanced parallel processing techniques. RTDS software is composed of accurate power system component models, which are used to represent complex systems. Digital and analog I/Os are used as interfaces and an amplifier is used as the actuator.

1.3 Thesis Organization

This thesis continues in Chapter 2 with an introduction to battery energy storage systems. It follows with the discussion about important battery parameters and models and different application of BES in power systems. Chapter 3 in-

troduces a widely used power electronic circuit to interface batteries to the grid. This chapter also describes controllers that are used. Chapter 3 also describes how DC-DC converters and voltage source converters (VSC) operate. Chapter 4 describes the case study and the setup used and discusses the results of simulation in PSCAD/EMTDC environment and in HIL simulation. Chapter 5 presents concluding remarks and contributions made in this research. Moreover the related subjects that can extend this research are proposed in this chapter.

2. BATTERY ENERGY STORAGE

Battery energy storage systems are used in applications where high-power-rating energy storage is required, e.g. in a hybrid electric vehicle (HEV) or in power system applications. In order to provide high power rating it is often required to have many battery packs in series and/or in parallel. Each battery pack is composed of individual battery cells. The series connection of cells yields a higher total battery voltage at the same capacity. The parallel connection yields a higher total battery capacity at the same voltage. Voltage level and capacity of a pack are defined by designer and vary in different applications [20].

Packs are equipped with cooling systems to prevent over-temperature of battery cells. In most practical systems packs are either water-cooled or air-cooled. Air or water is circulated in the pack to cool the battery cells. Cell temperature might increase as a result of chemical reactions inside them. Increase in temperature changes battery characteristics and in extreme cases might cause explosion of the battery pack. Thus temperature of each cell must be monitored constantly. Temperature sensor is used to monitor battery surface temperature and send information to battery management systems.

Usually battery management systems (BMS) are used to protect cells from undesirable operating conditions. They protect cells from over-temperature and over-current. In case of over-temperature or over-current the BMS usually disconnects the battery pack from the system through a main contactor although it constantly communicates with the main system to prevent this situation. By decreasing the pack current the temperture drops. A decrease in battery current slows down chemical reactions. Consequently the temperture decreases [21].

Data is constantly transferred between BMS and main control system. It includes cell voltages and temperatures, state-of-charge (SoC) and state-of-health (SoH) of battery cells. It also sends out battery current. It is common to use Controller Area Network (CAN) protocol for this purpose of communication. The CAN protocol is specially designed to tolerate noise and disturbances [22]. High frequency switching noise in power electronic devices is one of the motivations for the usage of this communication protocol in battery packs.

BMS usually controls contactors and the cooling system within a battery pack, e.g. when temperature rises the BMS locally decides to turn air-cooled cooling system on or when an over-current situation happens the BMS locally decides to open contactors to prevent any damage to the batteries.

When the battery is being charged, the BMS protects it from overcharging to ensure a long cycle life of the battery. When calculated SoC of a battery increases more than 100 percent or decreases less than 0-10 percent cycle life of a battery

decreases. The cycle life represents the number of cycles the battery can be charged and discharged before it is considered to be at the end of its life. A battery's end of life is when the capacity drops below a certain level, which is usually 80 percent of its nominal capacity. When a battery reaches its end of life, it still stores energy and is useful. The end of life term indicates that a battery might be no longer useful to be used in a system due to design criteria. For example in a system that requires 300kW of power, a BESS which can provide 240kW will not be meeting system requirements.

Depth of discharge (DoD) is also an important factor in capacity life of a battery. DoD is a measurement of the percentage of charge of a battery used in each cycle. For example if in each charge and discharge cycle of a battery, the SoC decreases from 80 percent to 40 percent and then charges back to 80 percent then DoD is equal to 40 percent. The DoD has an important effect on the cycle life of a battery. The smaller the DoD, the longer the cycle life [11].

Fig. 2.1 shows a sample battery pack. Each pack is connected to the next pack through contactors. These contactors let the system work without one specific pack. For example when a battery pack needs maintenance or repair and needs to be out of service, the rest of the system operates normally by bypassing that specific pack. Voltage of each cell and current of each pack will be monitored by the BMS. Fuses are also used to protect the pack from over-current. This is a physical protection in addition to the BMS system, which protects battery cells.

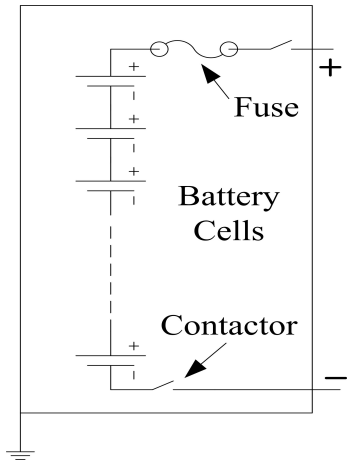

Fig. 2.1: A sample battery pack with multiple series batteries and fuse and contactors .

Grounding is also an important issue in the BESS. The chassis of battery packs are usually grounded. Especially in HEVs, the chassis of battery packs are connected to the chassis of the vehicle while positive and negative poles are isolated from the chassis. This provides safe operating conditions for operators. A floating chassis or connecting chassis to either poles is hazardous. For example in case the positive pole is connected to the chassis, if operator who is touching chassis contacts negative pole a short circuit situation happens through the operator's body.

BMS is also responsible of cell balancing. Differences between individual cells inside the battery pack cause an imbalance in the SoC of battery cells. Although cells inside a battery pack are in series and are supposed to have the same charge, that might not happen in reality. Manufacturing differences cause such difference. Cell balancing tries to level battery cell voltage in a pack either by charging cells

that have lower voltage or by discharging cells that have higher voltage. The former is called active cell balancing and the latter is passive cell balancing. In active cell balancing charge is sometimes transferred from cells with higher voltage to cells with lower voltage. Fig. 2.2 shows active and passive cell balancing methods. In comparison with passive cell balancing, active cell balancing is more efficient and is a faster balancing method [23]. Resistors are used to discharge extra cell charges in passive cell balancing. These resistors are usually mounted on the BMS board.

BMS also measures state of charge (SoC) and state of health (SoH) of a battery [24]. Methods to measure SoH and SoC of a BMS are discussed in this chapter. Sophistication of the BMS depends on its functionality. For example some of the BMSs only measure SoC and have no more functionality. In general, the higher the level of functionality of BMS, the better care will be taken of the battery.

BMS is composed of digital processors, I/O units and communication modules. I/O units are used to acquire data regarding voltage, temperature and current of each cell. Communication units are used to send SoC and SoH status to the main control system. The main control system is the unit, which organizes whole system if BESS is considered as a sub-system. For example in a HEV, the main control system controls the operation of internal combustion engine, batteries and electric motors. BMSs are provided with IP five or higher. The IP Code rates the protection degree against solid objects, dust and water in casings [25]. This high IP let BMS work in harsh environments.

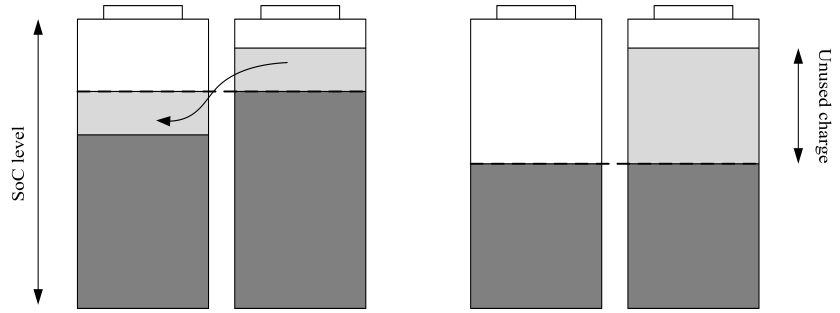

Fig. 2.2: Shows passive cell balancing on right and active cell balancing on the left .

2.1 Battery Characteristics and Specifications

Batteries are electrochemical devices that convert chemical energy into electrical energy by electrochemical oxidation and reduction reactions. These reactions happen at electrodes. A cell consists of an anode and a cathode. In the former, oxidation takes place during discharge while in the latter reduction happens. This means that the anode supplies electrons to the external circuit during charging. Electrolyte is the medium that provides ionic conductivity between positive and negative electrodes of a cell. Depending on the type of electrodes and electrolyte in the battery, the type and characteristics of battery change [26, 27].

Chemical reactions and characteristics of batteries are not the interest of this study, instead discovering information which are required to use batteries is the target, e.g. charge/discharge curves, methods to estimate SoC, restrictions on charge/discharge rates, energy to volume or energy to weight ratios, measurement methods of internal resistance or efficiency. With this information a battery can be used in system level design.

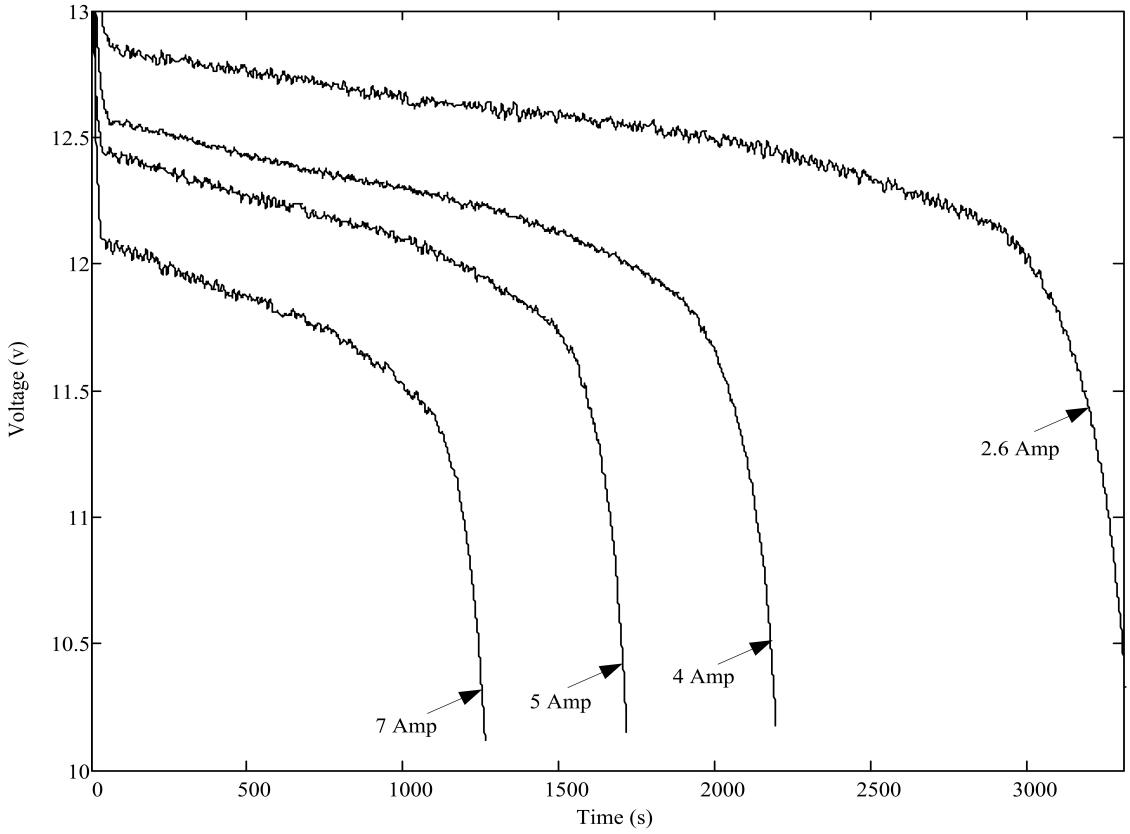

Fig. 2.3: Discharge curve of LPF26650P Lithium-Ion battery .

In this study high capacity LPF26650P K2 energy lithium ion battery (2.6Ah) and PC625 Odyssey Lead-acid battery (18Ah) are used. Battery manufacturers provide discharge curve of batteries. Fig. 2.3 shows voltage versus discharge time of a lithium ion battery for different discharge rates. To obtain these curves, the fully charged battery is discharged at different discharge rates. Discharge current is kept constant during discharge period. It is obvious that when the discharge rate is higher the battery voltage drops faster. The same thing happens when charging the battery. Battery voltage increases faster when the battery is charged with a

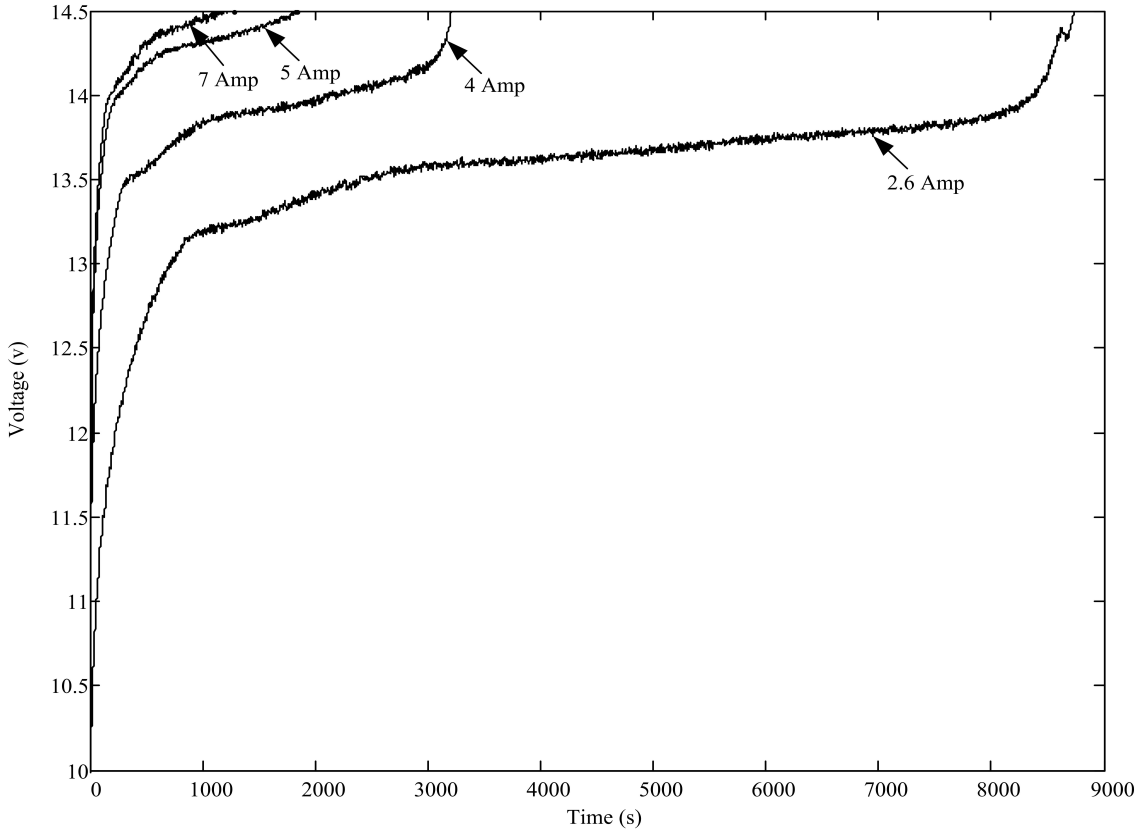

Fig. 2.4: Charge curve of LPF26650P Lithium-Ion battery.

higher current. Fig. 2.4 shows voltage versus charging time for different charge rates. Charging process is stopped when the terminal voltage reaches upper limit voltage indicated in the battery manual (14.5v in this case). When a battery is charged or discharged with higher current its capacity decreases this phenomenon is described by Peukert equation [28], as follows.

$$I^{pc}t = constant \tag{2.1}$$

In the Peukert equation I is the discharge current, t is the maximum discharge

time and pc is the Peukert coefficient(usually between 1 and 2). In lithium-ion batteries the Peukert coefficient is close to 1. In lead-acid batteries the Peukert coefficient is larger than in lithium-ion batteries. This means that discharge time decreases more significantly than li-ion battery when discharge current increases. Most battery manufacturers specify the capacity of their batteries for certain discharge time, e.g. C(20)=50Ah means that if it is discharged in 20 hours the capacity would be 50Ah. If it is discharged within a shorter time then the capacity could be calculated with Peukert equation. Fig. 2.5 shows that the available capacity of a battery decreases by increasing its discharge rate. This loss in capacity is temporary. After enough rest time full capacity will be available for use [28].

Energy density and specific energy are important factors in choosing battery type in different applications. Energy density and specific energy are expressed in Watt-hours per litre (Wh/l) and Watt-hours per kilograms (Wh/Kg). Fig. 2.6 and Fig. 2.7 depict energy density and specific energy in different battery types. In mobile applications such as hybrid electric vehicles batteries with high energy density and specific energy should be used. Lithium ion, lithium polymer and lithium phosphate batteries are presently the battery types with highest energy density in the market. These batteries are more efficient than most of the other types of batteries. On the other hand in standalone applications such as in uninterruptible power supply (UPS), batteries with low energy density can be also used. Lead acid

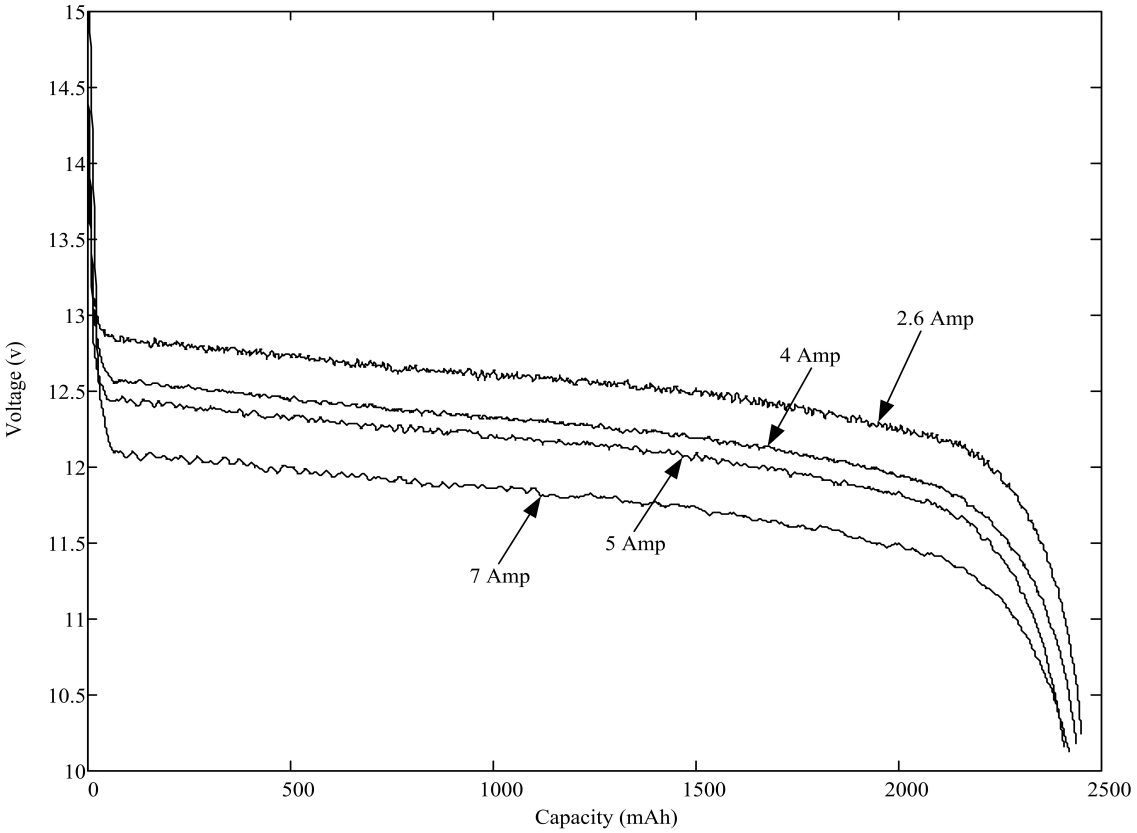

Fig. 2.5: Discharge curve of LPF26650P Lithium-Ion battery Versus capacity.

batteries have the lowest energy density among commonly used batteries in the market. Lead acid batteries are popular and have been used widely. They have previously dominated market because of ease in usage, maintenance and manufacturing. However low energy to weight ratio and energy to volume ratio of these types of batteries have reduced their popularity in mobile applications.

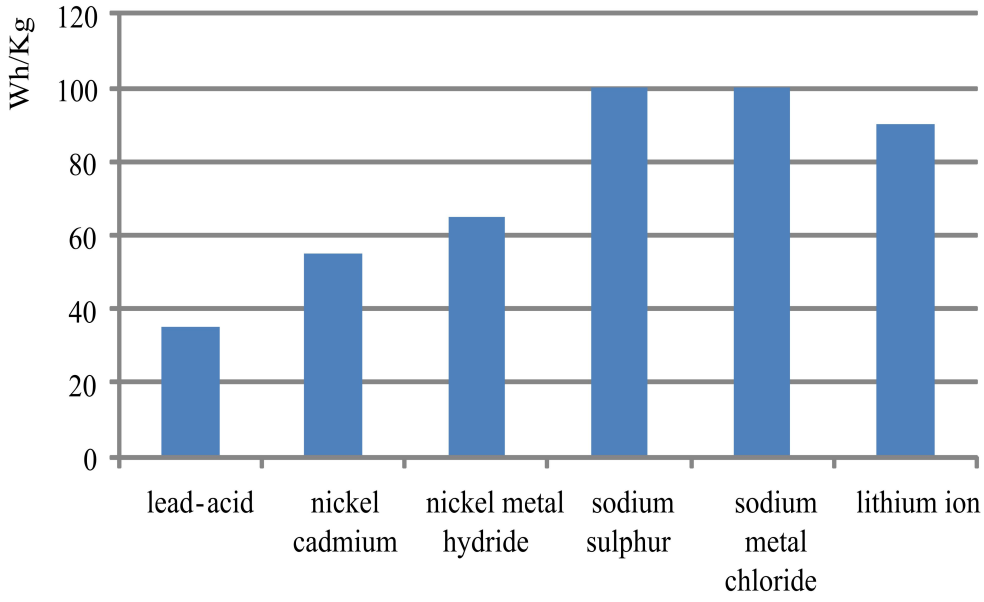

Fig. 2.6: Comparison of energy density in different battery types [1].

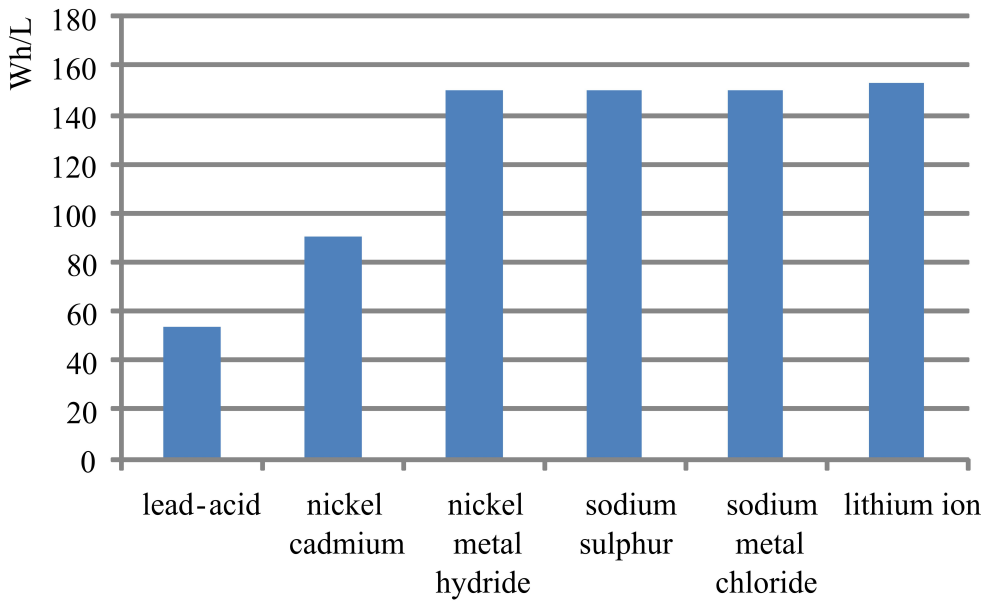

Fig. 2.7: Comparison of specific energy in different battery types [1].

2.1.1 State of Charge (SoC) and State of Health (SoH)

One of the most important parameters that is required for safe operation of a battery is the SoC. The SoC helps battery management and enables batteries to be safely charged and discharged. Precise SoC estimation prevents unpredicted system interruption and prevents battery from being over-charged or over-discharged, which may cause damage to its internal structure. In most applications, it is preferred to keep the SoC of the battery between 30 to 70 percent. This will increase battery life cycle time.

The SoC is defined as present capacity of battery expressed in terms of its rated capacity. Equation (2.2) shows a more accurate definition of SoC. It indicates that only releasable charge in the battery should be considered in the definition of SoC. In order to consider releasable charge, efficiency term should be used. Efficiency is defined and discussed in this chapter. By using the efficiency term η, equation (2.3) can be used as a replacement of equation (2.2).

$$SoC = \frac{Q_{releasable}}{Q_{rated}} \tag{2.2}$$

$$SoC = \eta \frac{\left(\int I(t)\, dt\right)}{Q_{rated}} \tag{2.3}$$

It is obvious that accumulation of current represents electric charge. By integrating charging and discharging current of the battery and multiplying by efficiency,

releasable charge will be available. Charging current should be considered positive as it increases charge level of battery. This tracking of SoC is called coulomb counting method. The coulomb counting method is widely used to estimate SoC in different battery types. One of the drawbacks of this method is accumulation of errors that piles up during operation time. Sensing elements such as Hall Effect sensors, which are used to measure current, might have some drifts. This error is accumulated during operation time. To compensate this error, voltage of batteries should be continuously monitored. When a battery is depleted its voltage drops. When voltage becomes less than a specific voltage the SoC can be assumed as zero. This value is usually mentioned in battery manuals. This method calibrates the coulomb counting estimation method [29].

Another common method of estimating the SoC is by measuring the open circuit voltage (OCV) of batteries. This method can be used for all type of batteries. The OCV should be measured after adequate rest time. This rest time varies for different type of batteries. For a lithium ion battery it can be measured almost immediately after disconnection of the load. In lead acid batteries a 5-minute rest time is essential. Fig. 2.8 shows OCV versus SoC for PC625 Odyssey lead-acid battery. Only OCV after a rest time is useful to estimate SoC.

As presented in Fig. 2.8 the OCV after rest time is linear and is a function of SoC. The OCV immediately after charging or immediately after discharging cannot be used to estimate the SOC. The OCV immediately after charging is more and

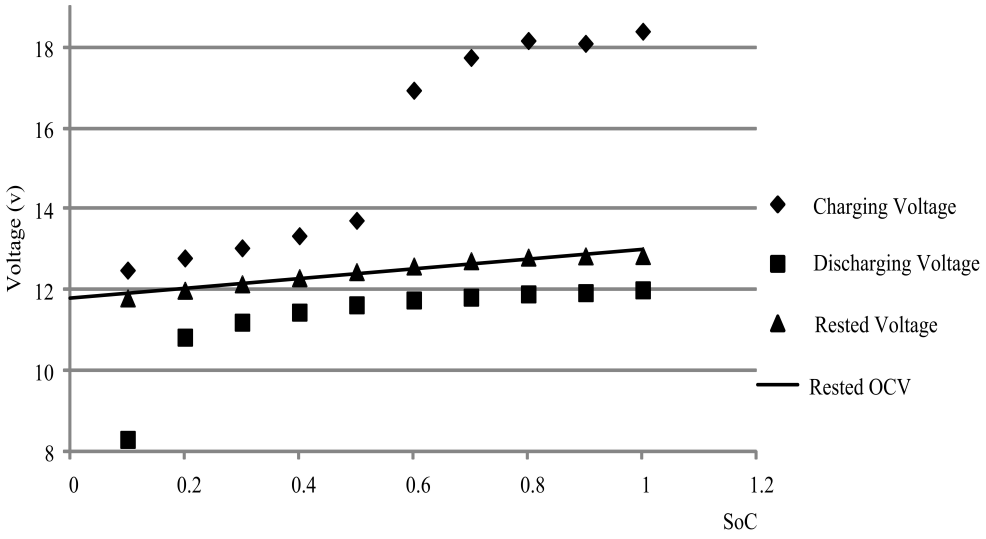

Fig. 2.8: Rested and Unrested OCV of PC625 Odyssey Lead-acid battery Versus SoC. Presented equation shows linear relation between OCV and SoC.

the OCV immediately after discharging is less than rested OCV. Rest time might vary for different type of batteries. During rest time chemistry of battery reaches equilibrium after disconnection from external circuit. Fig. 2.9 shows OCV versus SoC for different rest time after charge and discharge. OCV points after charge and after discharge get closer as time passes. For PC625 Odyssey lead-acid battery a 30 minute rest time is required to report the OCV in order to calculate SoC.

This method has less popularity in comparison to the coulomb counting method as batteries require a rest time before taking measurements. Batteries should be disconnected from load before measurement, which restricts usage of this method for SoC estimation. In addition, in some type of batteries such as lithium batteries, which have a horizontal linear section in their discharge curve, distinction between OCV might be difficult. For example the OCV of two point in discharge curve of

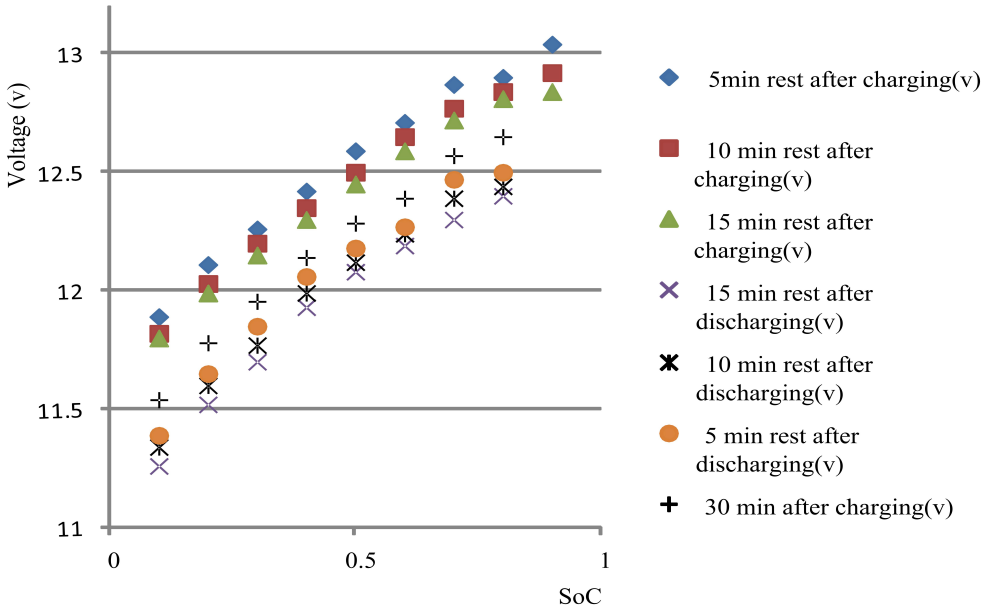

Fig. 2.9: Rested OCV of PC625 Odyssey Lead-acid battery with different rest time Versus SoC.

lithium batteries with 40 and 50 percent of SoC might be 0.1 Volts in difference. As this 0.1 volt might be comparable to accuracy of voltmeter, this might increase error in OCV method.

Maximum capacity of a battery might decrease during operation time. In that case maximum SoC of a battery would be less than one. For example an 18Ah battery might be only able to take 16Ah of charge. Any furthur attempt to increase battery charge would increase battery terminal voltage and is destructive to battery structure. A healthy battery is able to take its rated charge. In order to have an indication of the health state of a battery, the SoH is defined as in equation 2.4. Q_{Max} is maximum charge a battery is able to store. Q_{Rated} is rated capacity of battery.

$$SoH = \frac{Q_{Max}}{Q_{Rated}} \tag{2.4}$$

2.1.2 Efficiency

Efficiency is important in calculating the coulomb counting method, which was discussed in the SoC section earlier. A wrong efficiency figure causes large errors in SoC estimation over time. Efficiency changes by change in the SoC and/or charge and discharge rate. It is generally mentioned that battery charge efficiency is high at low SoC and decreases near full charge [30, 31]. Effciency of a battery also depends on the type of battery. No battery chemistry can obtain 100 percent energy efficiency, for the simple reason that there will always be energy dissipated as heat through internal impedances. In [29] efficiency of lithium-ion battery is reported around 99 percent for different discharge rates. In [30, 31] efficiency of lead-acid batteries is reported 30-90 percent depending on the operating condition. It also depends on the SoH of battery. Efficiency drops by increasing the number of the cycles a battery is used.

There are two commonly used definitions for efficiency in literature [27]. Energy efficiency is defined as the ratio of the available energy stored in a battery to the total energy used to charge the battery. In equation (2.5) $I_{Discharge}$ represents discharge current, I_{Charge} represents charge current and V_b shows battery voltage. This has the concept of energy loss embedded in it. In some references equation

(2.5) is replaced by equation (2.6). $R * I^2$ represents energy loss in the battery. R is the value of the internal resistance of battery. Although this is a good estimation for energy efficiency, it does not include the effect of temperature or the SoC in it.

$$\eta_{energy} = \frac{\left(\int V_b(t) * I_{Discharge}(t)\, dt\right)}{\left(\int V_b(t) * I_{Charge}(t)\, dt\right)} \tag{2.5}$$

$$\eta_{energy} = \frac{\left(\int V_b(t) * I_{Discharge}(t)\, dt\right)}{\left(\int V_b(t) * I_{Discharge}(t)\, dt\right) + R * I^2} \tag{2.6}$$

Coulomb efficiency is determined as the ratio of the electric charge that is discharged to the electric charge that should be charged to return battery to the same SOC. The experiment to determine coulomb efficiency is simple. Using a specific rate, the battery is first discharged to 10.5 V (for PC625 Odyssey lead-acid battery); this is the place where SoC indicator is reset to zero percent. It is then charged to a specific SoC, e.g. 50 percent. Equation (2.3) can be used to trace the SoC assuming η equals 1. This assumption will result in an error in the SoC calculation. Then the battery will be discharged until its voltage reaches 10.5V meaning the actual SoC is zero. The calculated SoC will not be zero as a consequence of wrong η. For example if the SoC indicator shows 10 percent at the end of the experiment, coulomb efficiency of this battery in that test condition would be 80 percent. Fig. 2.10 shows efficiency calculation method. This 80 percent should be used in charge the region. η for discharge region is considered

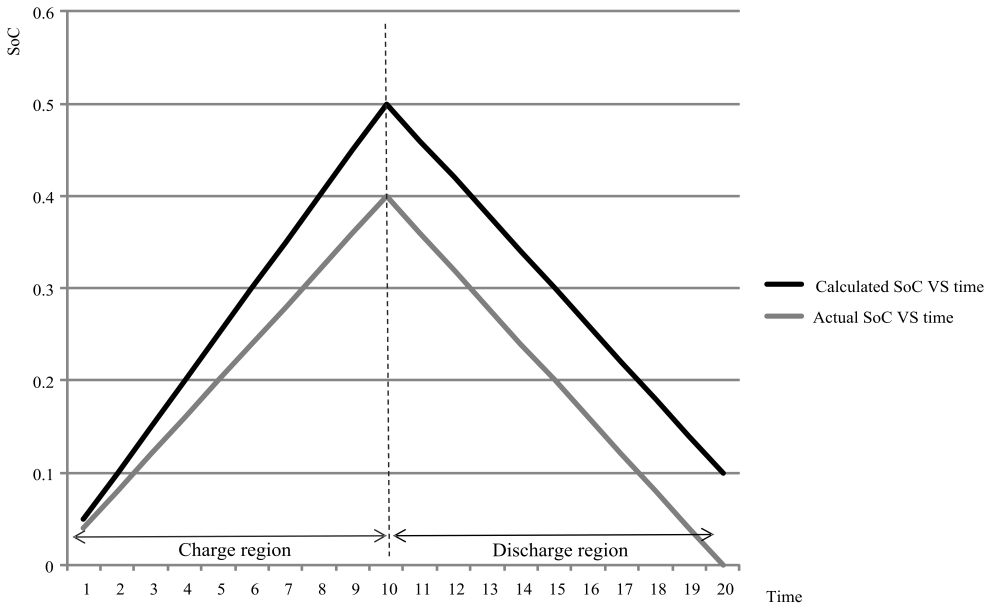

Fig. 2.10: Method to calculate efficiency.

as unity.

2.2 Battery Models

Testing batteries can be tedious, requiring many days and hours to complete simple tests. This is due mainly to the fact that batteries are electrochemical systems and in most tests a rest time is necessary before acquiring data. Simulation environments use battery models to analyze systems in short period of time. However, all models of batteries are unreliable at some level. The performance of a battery depends on quantities such as temperature and voltage. It also depends on parameters such as age, manufacturing tolerances and the way the battery has been used in the past. These variations in battery performance might not be considered

in battery models.

There have been several types of battery models [32, 33]. Electrochemical and empirical models are two main types of models that are used for modeling batteries. Empirical models are less accurate than electrochemical models but are widely used in simulation softwares. In order to extract required data from a battery cell, different methods are used. Electrochemical impedance spectroscopy(EIS) is commonly used to model battery cells. The EIS method uses the application of many sinusoidal waves that cover a wide range of frequencies. This method allows measurement of cell characteristics [33–38]. In EIS an ac current is imposed on an electrochemical cell and the potential across cell is measured. The experiment will be done for different frequencies and results can be presented using equivalent circuit elements [39, 40].

Thevenin model or ideal model, Randle model, and Shepherd model are common models studied in this thesis. These models are presented using equivalant circuit elements.

2.2.1 Thevenin Model

Thevenin model or ideal model is the simplest model used in this context. It is composed of a voltage source and a resistor. Fig. 2.11 shows an ideal battery model. The voltage source represents the OCV of a battery. The resistor resembles the internal resistor of a battery. The value of voltage source and the resistor depend

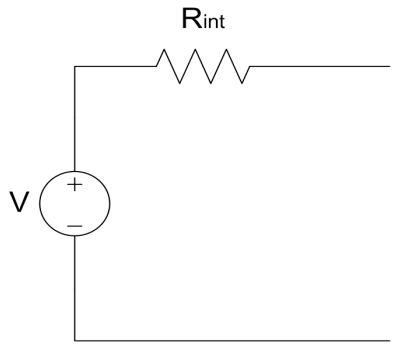

Fig. 2.11: Thevenin or ideal battery model.

on battery cell. In order to use this model the resistor value must be measured [41].

Although this battery model is simple to use it is not accurate. The value of the open circuit voltage of a battery depends on temperture and also the SoC. The value of the resistor also depends on the SoC, the SoH and the temperture of a battery. Assuming fixed value for the OCV and the resistor makes the model inaccurate.

Internal resistance of a battery changes by change in temperture and SoC of a battery [42]. Fig. 2.12 shows measured internal resistance of PC625 Odyssey lead-acid battery versus SoC. Internal resistance is higher when battery is depleted and decreases as state of *c*harge of battery increases. To measure internal resistance of a battery a specific current will be imposed to charge the battery. Due to internal resistance of a battery, terminal voltage of battery increases. Difference of voltage level of battery over injected current results in internal resistance of battery. For example in Fig. 2.13 charging current is five Amperes and increase in

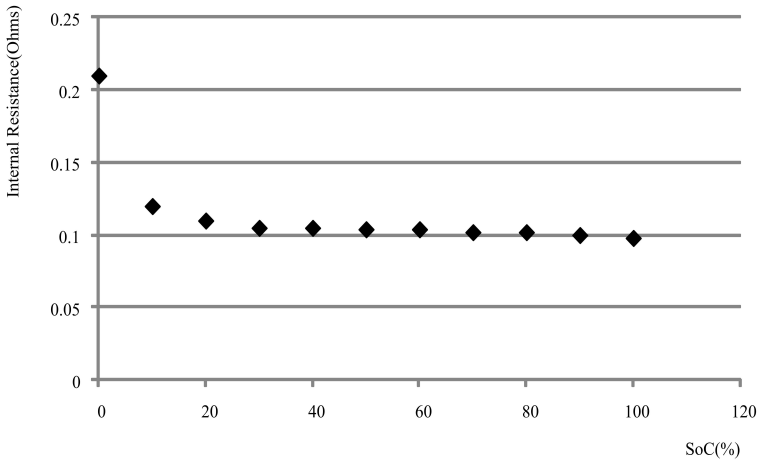

Fig. 2.12: Internal resistance vs state of charge.

battery terminal voltage is 1.5V. This yields 0.3 Ω as the internal resistance.

Value of internal resistance of a battery is also used to measure SoH of a battery. Internal resistance of a battery increases when battery is aged.

$$R_{int} = \frac{\Delta V}{I_{charge}} \tag{2.7}$$

2.2.2 Randle's Model

As shown in Fig. 2.14 Randle's model has two resistors and a capacitor. The values of these elements can be defined by using a curve fitting method. In that method, values of resistances and capacitor are defined in a way that the model and actual battery have the same discharge curve [43]. Another method to obtain parameters is by extracting information from an experiment. Fig. 2.15 shows an experiment to determine values of resistances and the capacitor. When the capacitor is fully

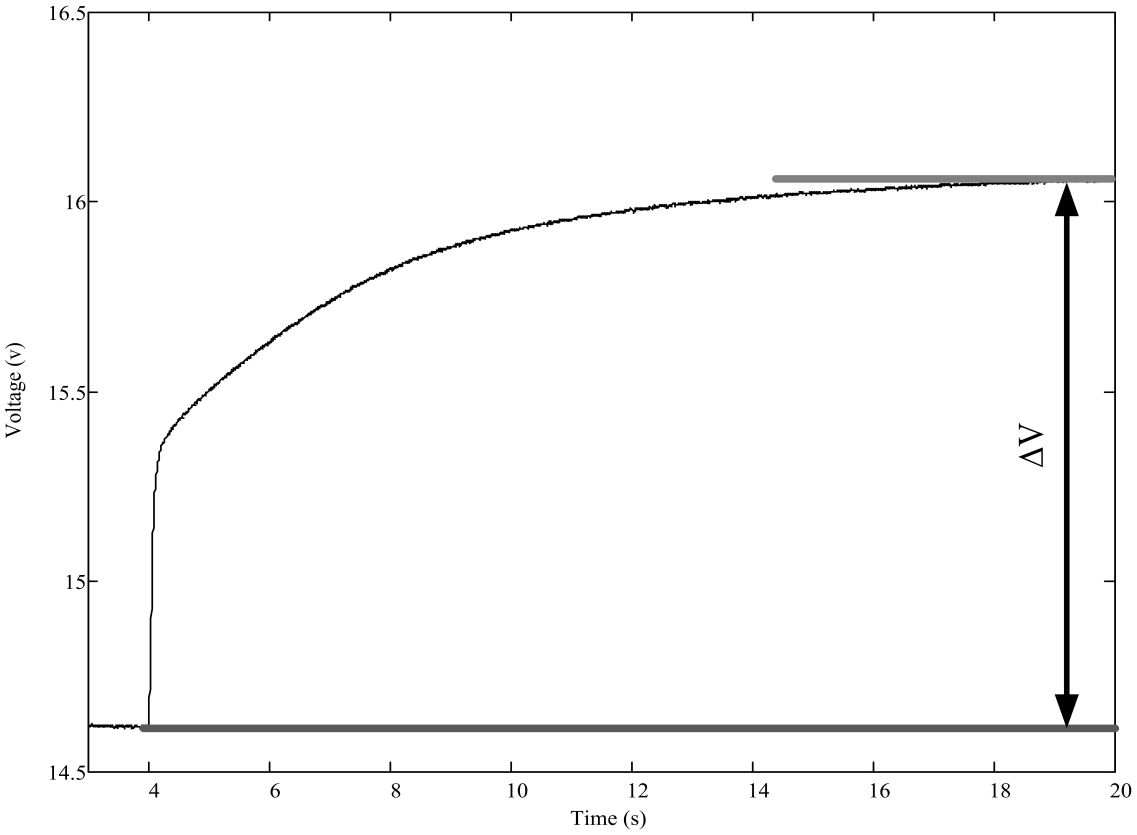

Fig. 2.13: An experiment to measure internal resistance of battery.

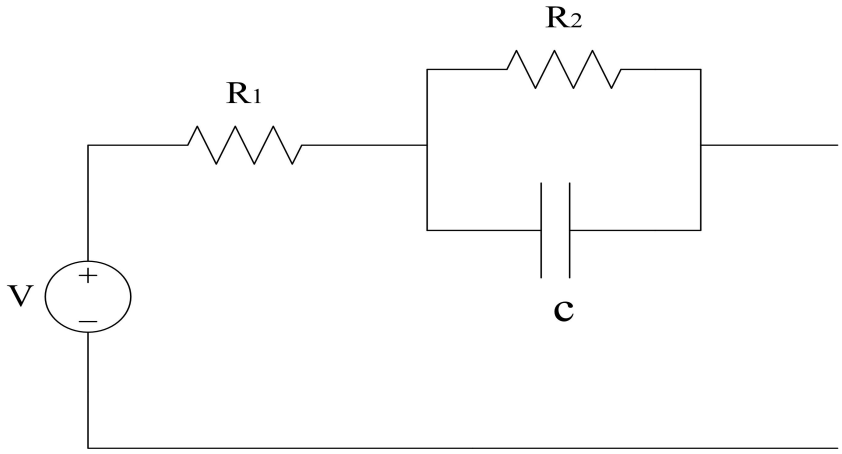

Fig. 2.14: Randle's model.

charged charging current passes through R_1+R_2. This causes a potential difference of ΔV_1 after response has settled. When capacitor is fully discharged, the charging current passes through R_1. This causes a potential difference of ΔV_2 short after charging current is applied. The value of R_2 is the difference of two values obtained above. The value of capacitor is defined using the time constant of the response.

$$R_1 + R_2 = \frac{\Delta V_1}{I_{charge}} \tag{2.8}$$

$$R_1 = \frac{\Delta V_2}{I_{charge}} \tag{2.9}$$

$$R_2 = \frac{\Delta V_1}{I_{charge}} - \frac{\Delta V_2}{I_{charge}} \tag{2.10}$$

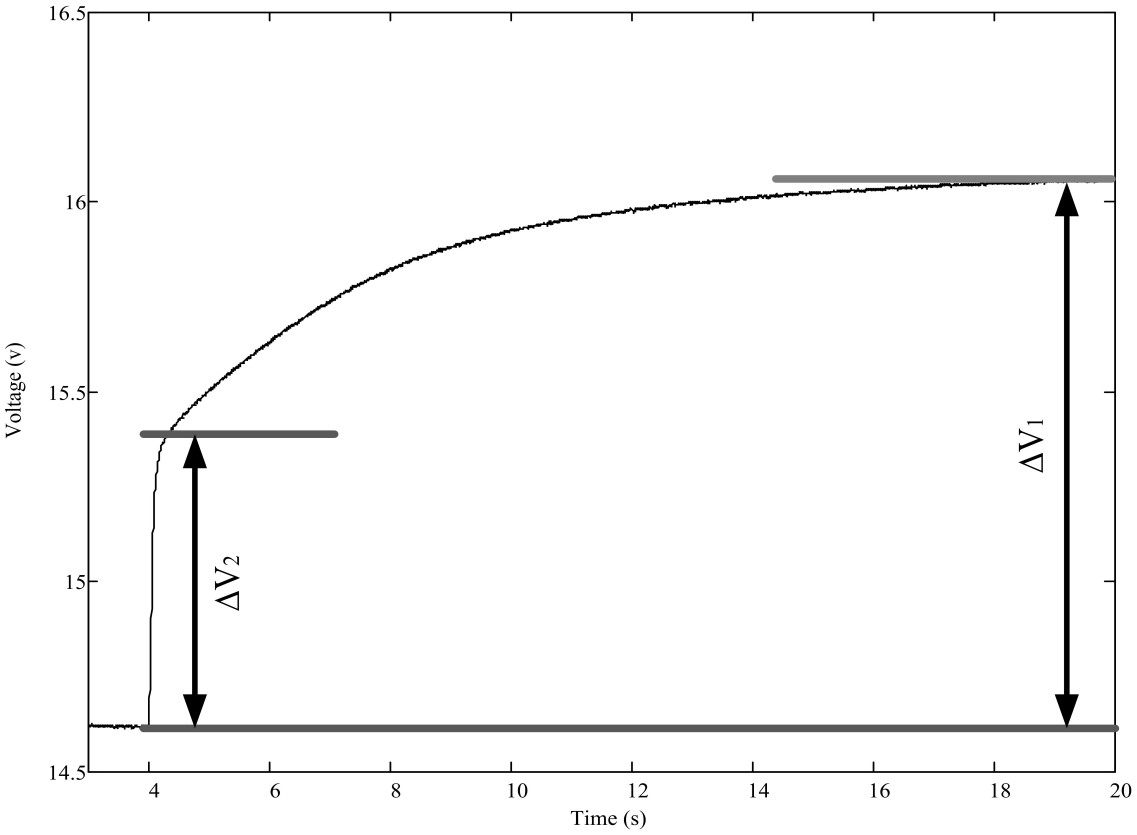

Fig. 2.15: An experiment to measure Randle model's parameters.

2.2.3 Shepherd Model

Shepherd Model was developed in 1960's to model a battery [44]. It is composed of a variable voltage source and a resistor. The value of the resistor should be measured by doing an experiment on the battery. The value of variable voltage source is determined by Equation (2.11). The values of A,B and K in Equation (2.11) are defined in equations (2.12),(2.13),(2.14). V_0 is nominal voltage and Q is battery capacity value in Ah. Values of V_{Exp}, Q_{Exp}, V_{Nom}, Q_{Nom}, V_{Full} are defined by extracting information from a discharge curve of the battery at 0.2C discharge rate [45, 46]. Fig. 2.16 and Fig. 2.17 show validated Shepherd model for PC625 Odessey lead-acid and also LPF26650P K2 Energy lithium-ion batteries.

$$V = V_0 - K\frac{Q}{Q - \int i(t)\,dt} + A\exp\left(-B\int i(t)\,dt\right) \tag{2.11}$$

$$A = V_{Full} - V_{Exp} \tag{2.12}$$

$$B = \frac{3}{Q_{Exp}} \tag{2.13}$$

$$K = \frac{(V_{Full} - V_{Nom} + A(\exp(-BQ_{Nom}) - 1)).(Q - Q_{Nom})}{Q_{Nom}} \tag{2.14}$$

For this study Thevenin, Randle's and Shepherd models are considered for high

capacity LPF26650P K2 Energy lithium ion battery(2.6Ah) and PC625 Odyssey lead-acid battery(18Ah). Figures (2.16,2.17) show actual and simulated discharge curves at discharge rate of 0.2C for batteries used in this thesis.

The Thevenin model is easy to implement. It does not need much information except that in the manual provided by the manufacturer. Randle's model is more acurate than the Thevenin model. It considers the dynamics of battery. On the other hand it uses a constant voltage source, which makes the model somewhat inaccurate. The OCV changes by change in SoC and it is considered in Shepherd model. Shepherd model is one of the most common battery models and is used in many software environments. Figures (2.18,2.19,2.20) compare all three battery models discussed in this chapter with actual test result. Test begins at SoC of zero and is charged gradually. Battery is charged for certain time and then a rest time is provided. Since in rest period no current passes the internal resistance of the battery, a voltage drop occurs on the battery terminal voltage. This test shows that Shepherd model follows actual battery as the OCV of this battery model is not constant. On the other hand Thevenin and Randle's model are far away from actual behavior of the battery in some operating regions. When the SoC of the battery is low the difference between actual and Thevenin model is more and it reduces when SoC increases.

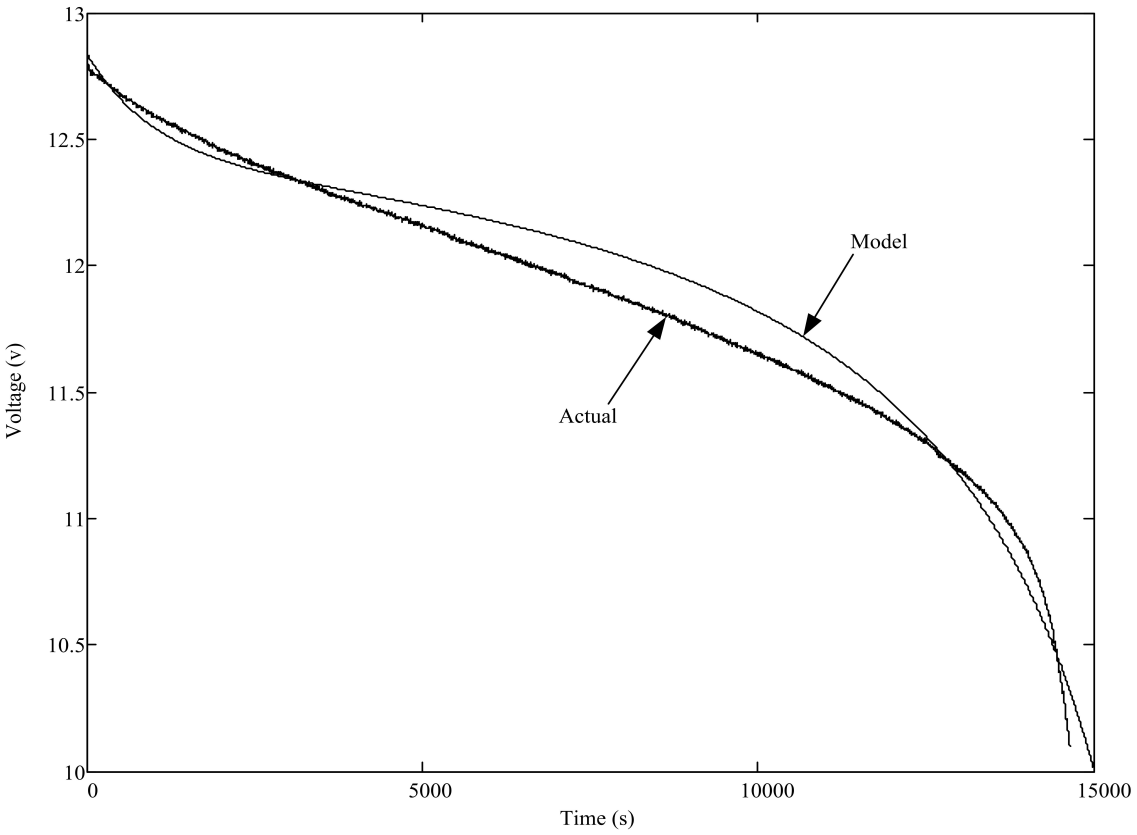

Fig. 2.16: Actual and Shepherd model discharge curve for PC625 Odyssey lead-acid battery.

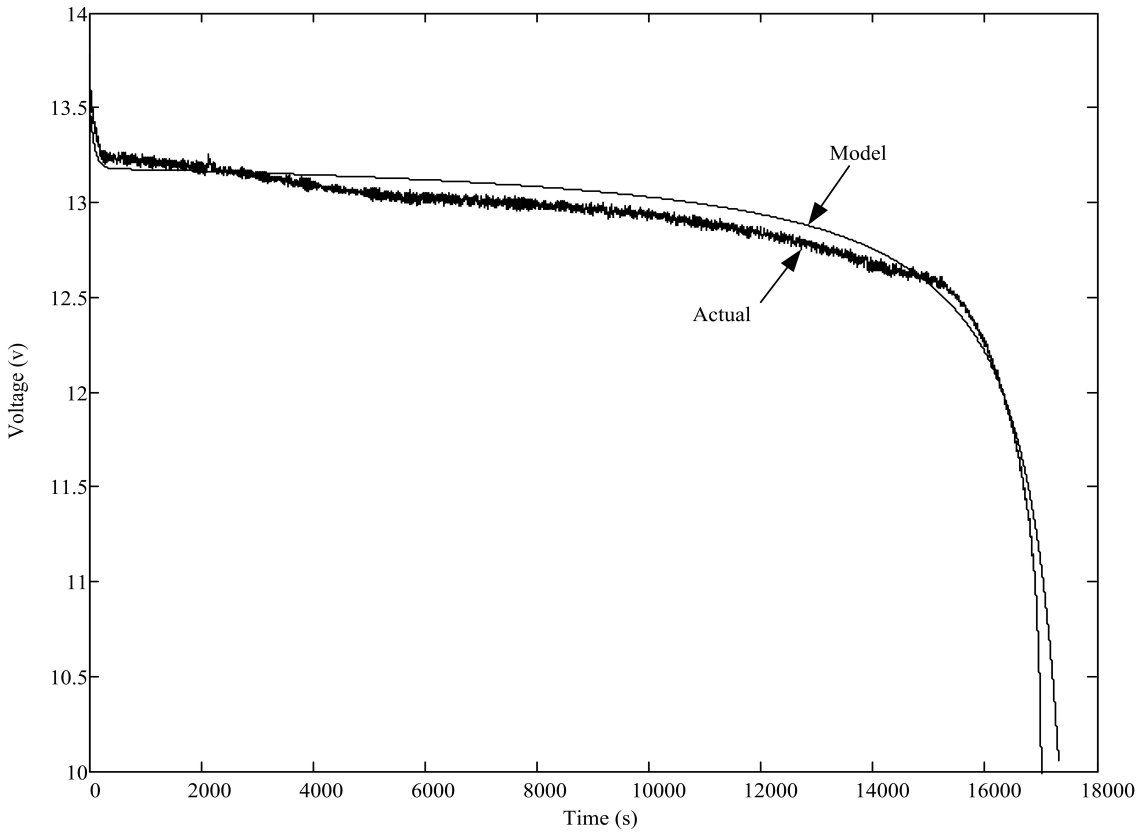

Fig. 2.17: Actual and Shepherd model discharge curve for LPF26650P K2 energy lithium ion battery.

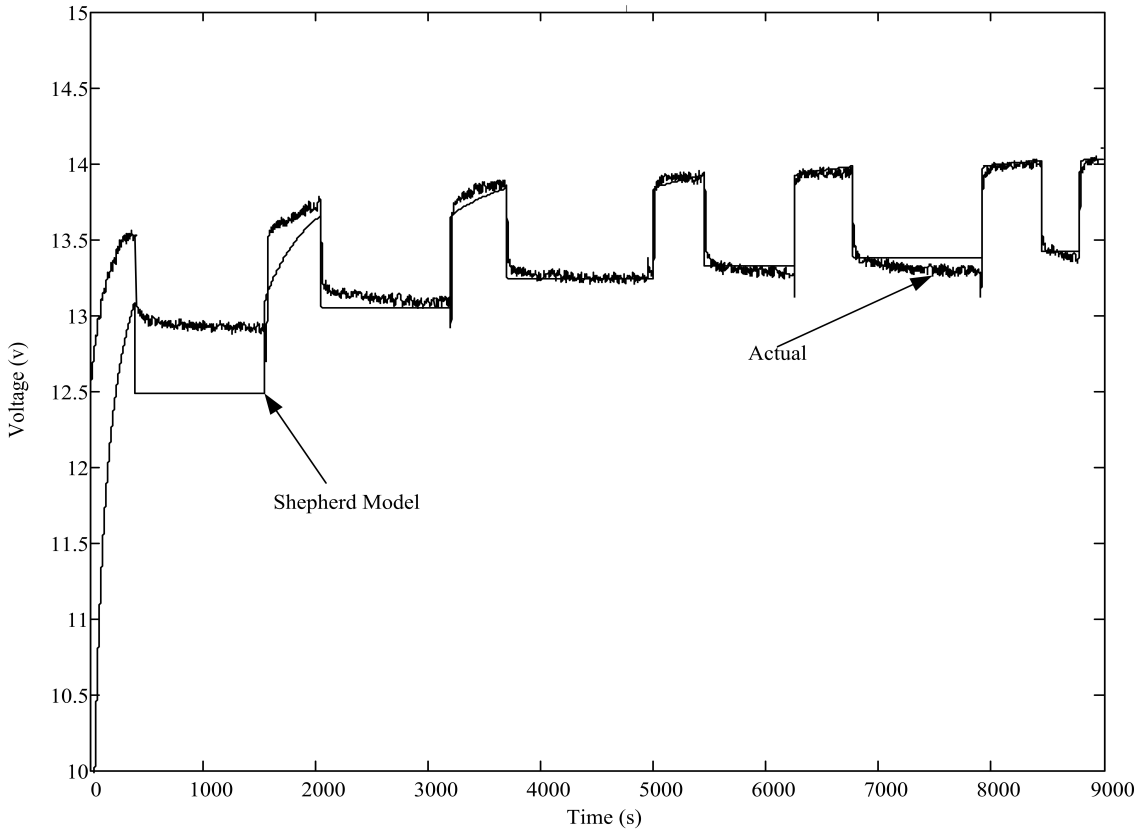

Fig. 2.18: Comparison of Shepherd model and a real battery in pulsed charging process.

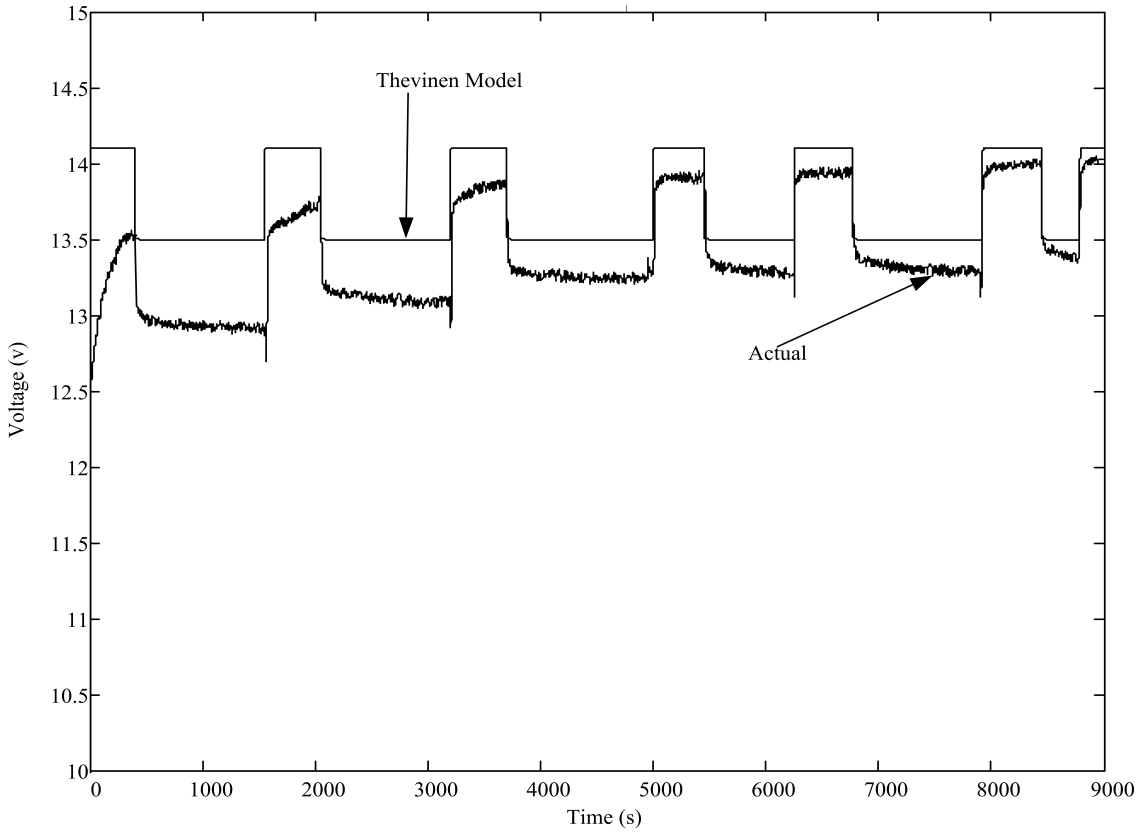

Fig. 2.19: Comparison of Thevenin model and a real battery in pulsed charging process.

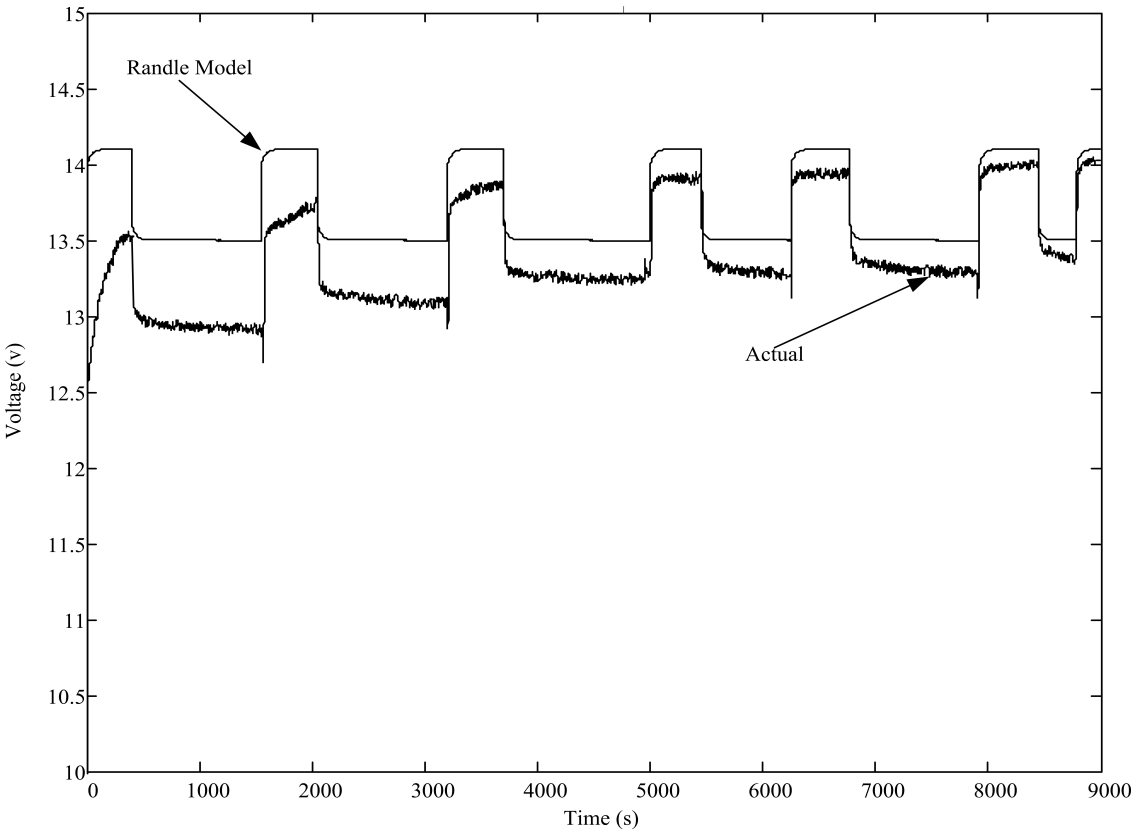

Fig. 2.20: Comparison of Randle model and a real battery in pulsed charging process.

2.3 BES in Power Systems

The need for storage devices and their usage in power systems has been studied in [47–49]. BESS, pumped hydropower, compressed air energy storage, flywheels, super capacitors, hydrogen storage are some of the technologies used to store energy in power systems. Table 2.1 shows that different types of batteries are used in power systems.

In [49] use of battery energy technology to improve power quality and reliability of the power system are discussed. BESs are also used in micro grids specially during the non-availability of the power grid. In this usage they serve the system as back up power source.

One of the other usages of BES is in renewable energy sources. Most of the renewable energies used in generation plants are solar and wind energy. The main disadvantage of these kinds of renewable energy is their generation intermittency, as well as the fact that their energy generation is not controlled. Energy storage systems can solve the problems described above. A renewable energy generation plant with its corresponding energy storage system can behave as a constant power generation plant.

There are two reasons for limited practical application of batteries in power systems. Firstly, conventional power system have large amounts of generating sources whose generation could be easily varied to match the load demand. Most of systems are interconnected and power from generators in other areas can be used

Tab. 2.1: Different Battery Types in Power Systems

Battery type	Largest capacity	Location
Lead Acid	10 MW/40 MWh	California-Chino
Lead Acid	300 kW/580 KWh	Milwauke,Wisconsin
Nickel cadmium (NiCd)	27 MW/6.75 MWh	GVEA,Alaska
Sodium sulphur (NaS)	9.6 MW/64 MWh	Tokyo,Japan
Vanadium redox (VRB)	1.5 MW/1.5 MWh	Japan

to balance the load demand. Consequently conservatives in the power industry try not to rely on BESS. Secondly, high capital cost of BESS is one drawback of their usage. In spite of these drawbacks, different battery types are practically used as BESS. Table 2.1 shows different BESS used in some of the projects.

In this chapter important characteristics of batteries were reviewed. Methods to estimate SoC were discussed. Finally, three types of battery models were developed and verified.

3. BESS IN WIND FARMS

Using BESS in a renewable energy application needs appropriate power electronics. Power electronic devices serve the BESS as an interface. This interface connects the BESS to other subsystems. The required power electronics vary in different renewable energy applications. For example power electronic devices that are used in solar sites are different from those used in a wind farm. In wind applications the type of power electronics also depends on the type of wind farm and configuration of farm in which the BESS is used. This chapter discusses the necessity of BESS in wind applications, how it is connected to a type 1 wind farm, and the type of power electronics it requires.

3.1 Wind Power

Importance of wind energy is increasing throughout the world. Wind energy is a growing energy technology. The production of large-scale, grid-connected wind turbines has doubled almost every three years [3]. Wind turbines use the wind energy close to the ground. The wind speed varies as a function of time and height. Wind turbulence, diurnal and synoptic speed variations have contributions

to change of wind speed. Turbulence is caused by gusts in the range of a fraction of second to a few minute. From a power system point of view, turbulence affects power quality of wind power production. Power quality degrades as the produced active power is not constant as a consequence of change in wind speed. A large penetration of wind generation in power system means that poor power quality and poor stability margins cannot be tolerated from wind farms. This requires methods to improve power quality and stability of wind farms. One of the methods to improve power quality is by keeping the produced active and the consumed reactive power constant.

The power of the air mass that flows at speed V through an area A can be calculated from equation (3.1). P_{Wind} is in Watts, $A(m^2)$ is the area , $V(\frac{m}{s})$ is air speed and $\rho(\frac{kg}{m^3})$ is air density in equation (3.1). Air density is a function of air pressure and air temperature, and consequently is a function of height [3].

$$P_{Wind} = \frac{1}{2}\rho A V^3 \tag{3.1}$$

The power of wind cannot be completely converted to mechanical power. Betz discovered that the maximum energy that can be harvested from wind power is 59 percent of the total energy of wind [3]. This is expressed in equation (3.2).

$$P_{Betz} = \frac{1}{2}\rho A V^3 C_{PBetz} = \frac{1}{2}\rho A V^3 * 0.59 \tag{3.2}$$

Practical harvested power depends on power curve of a wind turbine. It is a relationship between wind speed and harvested power. At wind speeds less than the cut-in speed no power will be produced. At wind speeds higher than the rated wind speed, the maximum power production will be limited. In region beyond rated speed, pitch-control or stall control techniques regulate the output power. In this area a constant output power is provided. At speeds more than the cut-out wind speed turbine stops power production. If wind speed goes beyond the cut-out speed, wind turbine stops power production. For example power production may stop during a storm. This is a problem especially in networks with high penetration index of wind power. To reduce this problem some manufacturers offer wind turbines with power curves that reduce power production step by step as wind speed increases. This reduces possible negative impacts of sudden shutdown of large wind power.

Figures 3.1 depicts how the change in wind speed changes the output power of wind turbine. This is part of the case study of this thesis. In this scenario a 1.32 MW wind turbine is connected to an induction generator with the same ratings at 690V line to line voltage. The structure of case study will be discussed later in this chapter. As wind speed goes beyond rated wind speed angle of blades of turbine change to regulate the output power. The pitch mechanism is not fast enough to avoid such power fluctuations. By using pitch control method, slow variations in the wind can be compensated, but this is not possible in the case of gusts. BESS

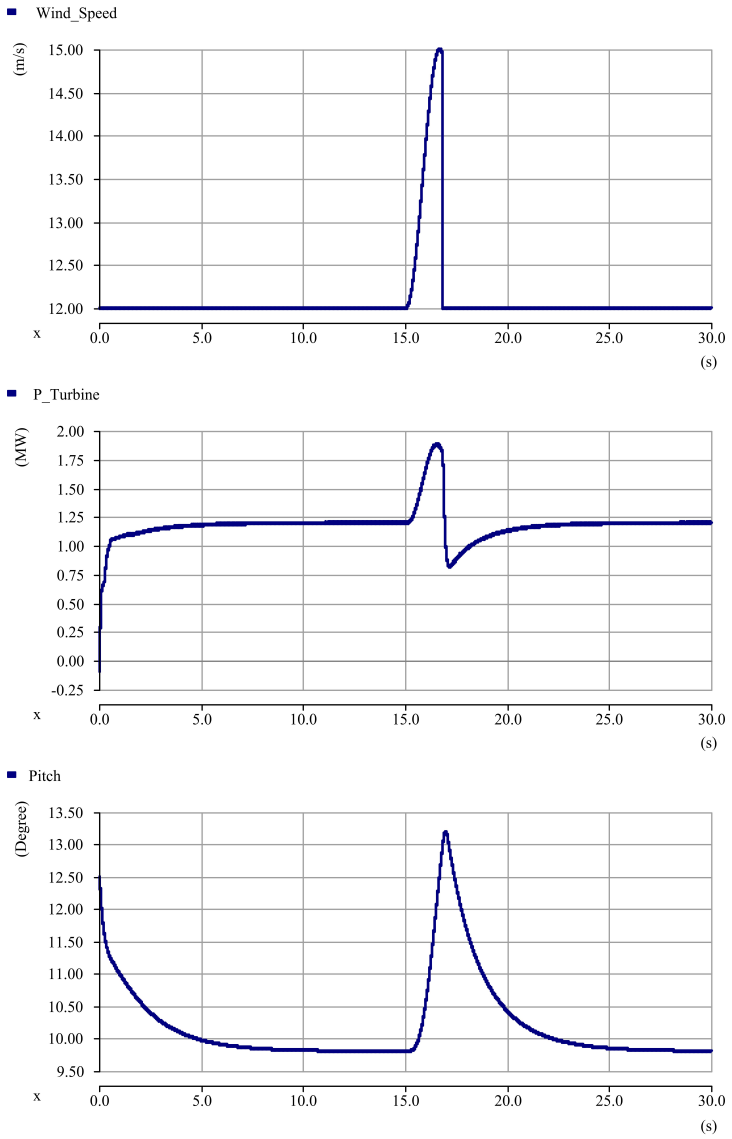

Fig. 3.1: Effect of change of wind speed in wind power, figure on the top shows wind speed vs time, the one at the middle shows wind power VS time and the last figure shows angle of pitch vs time.

are used to keep output power of farm constant. When wind power production is less than the expected value, the BESS produces power and when is more than rated value the BESS stores the extra energy.

To describe wind speed behavior, it is common to describe the wind speed pattern in the form of a probability density function (pdf). Equation (3.3) is a general expression that is often used for characterization of wind speed and is called the Weibull probability density function [3].

$$f(v) = \frac{k}{c}(\frac{v}{c})^{k-1} exp^{-(\frac{v}{c})^k} \tag{3.3}$$

In Equation (3.3) k is called shape parameter, and c is called scale parameter. For $k = 2$, Weibull represents a more realistic curve for wind speed than with other values of k [3]. This distribution is called Rayleigh probability density function. Equation (3.4) shows the Rayleigh pdf. Rayleigh pdf with an average speed of $12\frac{m}{s}$ is used to generate wind speed profile in HIL simulation of this thesis. Value of c is determined by equation(3.5) [3]. $V_{average}$ indicates average speed of the wind.

$$f(v) = \frac{2v}{c^2} exp^{-(\frac{v}{c})^2} \tag{3.4}$$

$$c = \frac{2\,V_{average}}{\sqrt{\pi}} \tag{3.5}$$

3.2 Configuration of Type 1 Wind Farm

In a type 1 wind farm an asynchronous squirrel cage induction generator (SCIG) is used. It is directly connected to the grid via a transformer. Capacitor banks are used for reactive power compensation as the SCIG draws reactive power from the grid. It is an electrical component that supplies reactive power to SCIG. Thus the reactive power absorbed by the generator from the grid reduces [3].

A soft-starter is usually used for smoother grid connection. The soft-starter reduces the in-rush current. In-rush current can be up to 7-8 times the rated current and can cause severe voltage disturbances on the grid. The soft starter is composed of two thyristors in each phase. One of the thyristors is in reverse to the other thyristor in each phase [3]. The soft starter connects the generator to the grid smoothly. This process is achieved by adjusting the firing angle of thyristors. Figure 3.2 shows schematic of a typical type 1 wind farm. Other type of wind farms are discussed in [3].

Wind fluctuations are converted into mechanical fluctuations and then into electrical power fluctuations. A proper control scheme in the wind energy generation system is required to allow proper control over the active power production. A battery energy storage system for wind energy generating system is generally required to compensate the fluctuations generated by wind turbine. The static synchronous compensator (STATCOM) with hybrid battery energy storage has great potential to play this role. The STATCOM is used to compensate the reac-

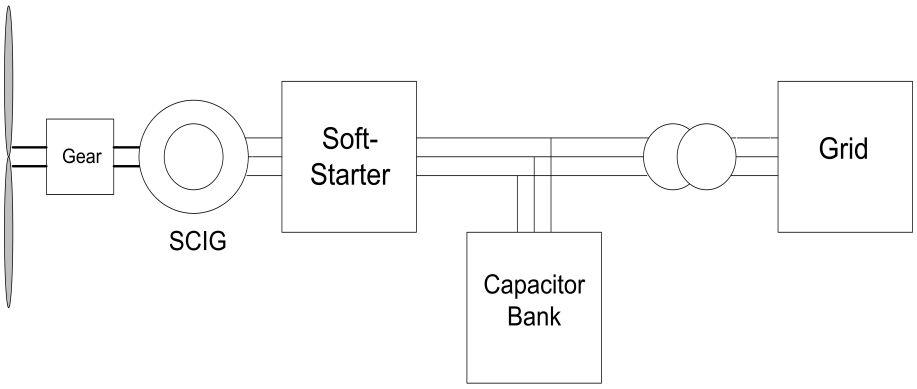

Fig. 3.2: Schematic of a typical type 1 wind farm.

tive power in a grid. It is a three-phase voltage source inverter having a capacitor on its DC link and connected at the point of common coupling [7]. BESS maintains DC capacitor voltage constant. In this thesis the BESS is connected in parallel with a capacitor to the DC side of a three phase voltage source inverter with the purpose of control of the active power. It is similar to a STATCOM with BESS in physical structure and appearance. Figure 3.3 shows schematic of STATCOM with a BESS.

3.2.1 BESS Sizing

Battery capacity is normally specified in terms of both power and energy capacity. The energy capacity describes the energy that can be drawn from or stored in the battery and is in kWh. The power rating determines the power that can be supplied or stored by the battery. Cost of the battery can also be determined, based on the power and energy capacities [50]. Figure 3.4 shows power variation of wind turbine

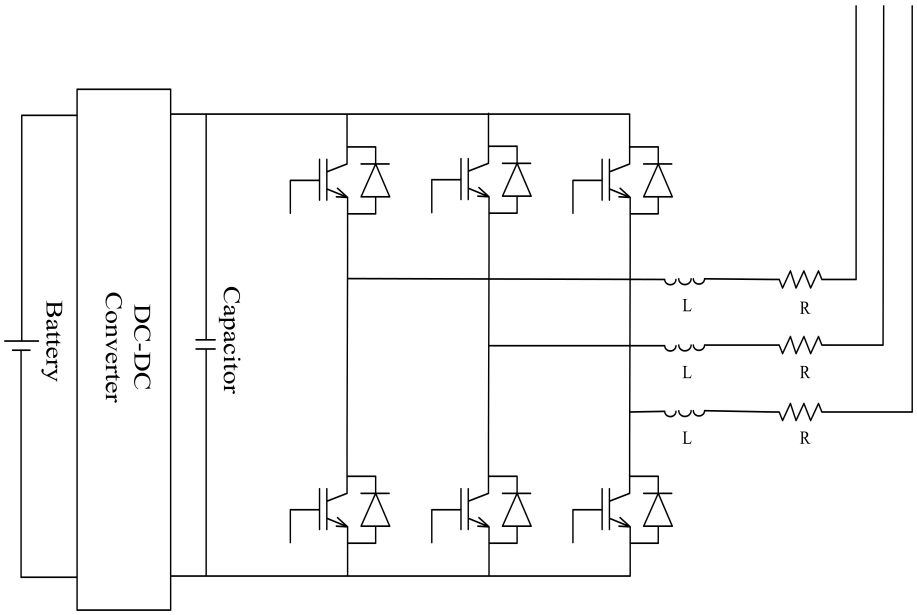

Fig. 3.3: STATCOM with hybrid battery energy storage.

in case study of this thesis. Energy of area 1, which is above expected power should be stored in BESS. Average output power in this simulation is 1.25MW. Energy of area 2, which is below expected power should be compensated by BESS. The highest peak of area 1 shows the maximum power that should be provided by the BESS. The lowest peak of area 2 shows the maximum power that should be harvested by BESS. In this thesis it is assumed that battery terminal voltage is 12 volts and current is limited to 10A. Consequently each battery provides 120W. For compensation of 1.32MW of variation in power 344 packs should be used in parallel. Each pack should be composed of 32 batteries in series. For the purpose of HIL simulation in this thesis a scaled HIL method is used. This will be discussed in the next chapter.

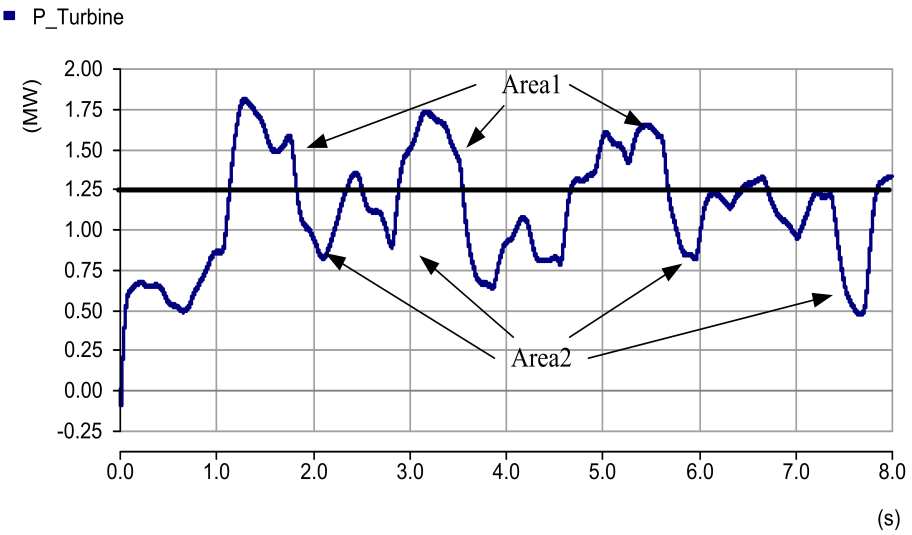

Fig. 3.4: Sample power variation of wind.

3.3 DC-DC Converter

For the purpose of connection of the BESS to the DC link of a STATCOM, it might be required to change the battery voltage level. For example if the DC link voltage is 1600V and BESS terminal voltage is 300V, the BESS voltage needs to boosted up. Power electronic devices are required to connect the batteries to a higher voltage level. Power electronics is a technology that converts electric power from one form to another. Power electronic converters can be classified into four different types on the basis of input and output, DC-DC, DC-AC, AC-DC, and AC-AC. DC-DC converters are usually used to change voltage level of input to desired output voltage level. Figure 3.5 shows the DC-DC converter, which is used in case study of this thesis. It is used to increase the BESS voltage level. It is composed of two diodes, two controlled switches, two capacitors and an inductor.

It is a bidirectional converter, which is able to transfer power from either side to the other. One side of the converter will be connected to the BESS and the other side is connected to the DC link of the VSC. When switch S1 is enabled switch S2 is turned off and the parallel diode D2 is in the circuit. The duty cycle of switch S1 is defined as in equation (3.6). It is the ratio of the on-time of the switch to the period time of switching. The duty cycle is an important control parameter in power electronic circuits. Relation between V1 and V2 is defined in equation (3.7) when switch S1 is enabled. This equation indicates that voltage level of V2 is a function of V1 and the duty cycle of switch S1. In this case it is possible to transfer power from V2 to V1. If the BESS is connected to V1 side this mode will be the charging mode.

On the other hand when switch S2 is enabled and switch S1 is turned off, diode D1 is in the circuit. Relation between V1 and V2 is shown in equation (3.8). In that mode power is being transferred from V1 side to V2. If BESS is connected to V1 this operating mode would be discharging mode.

$$Dutycycle = \frac{T_{on}}{T} \tag{3.6}$$

$$V_2 = \frac{V_1}{D_{S1}} \tag{3.7}$$

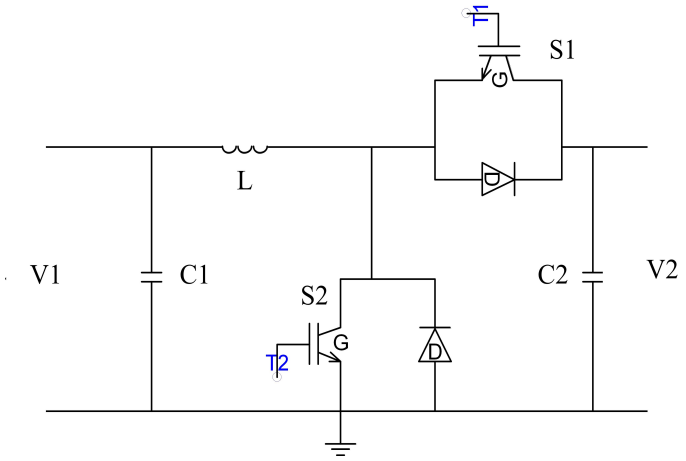

Fig. 3.5: A Bidirectional converter.

$$V_2 = \frac{V_1}{1 - D_{S2}} \tag{3.8}$$

In battery applications it is important to have control over charge or discharge current of batteries. Charge or discharge currents that are more than the rated values indicated by manufacturer would cause serious damage to battery. To protect battery from over-current, the value of the duty cycle is calculated through a simple proportional-integral (PI) control strategy. The schematic diagram of the control algorithm is depicted in Figure 3.7. The value of current is compared with the desired current and the appropriate duty cycle will be calculated at the output of the PI block. Duty cycle is a value between zero and one. To build firing pulses of switches a constant value is compared with a periodic ramp. The ramp varies from zero to one. If the ramp value is more than the constant value firing pulse is zero, otherwise it is one. Figure 3.6 shows how firing pulses are

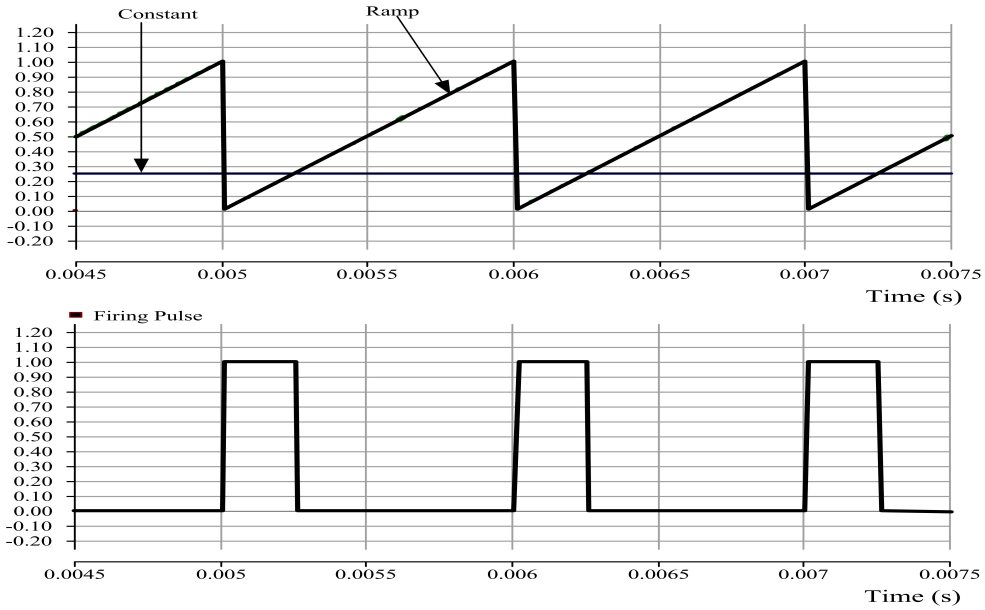

Fig. 3.6: Duty cycle generation.

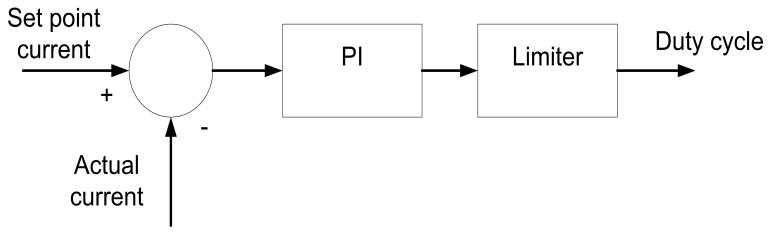

Fig. 3.7: Control block diagram of DC-DC converter.

generated. In Figure 3.6 a ramp signal with a frequency of 1 kHz is compared with a constant value of 0.25. Firing pulses also have the same frequency as the ramp. In the case study the change of the duty cycle changes the voltage of the battery terminal. Consequently current that passes through the battery changes. Battery terminal voltage changes during the charge or discharge process. To keep charging or discharging current constant the duty cycle should change accordingly.

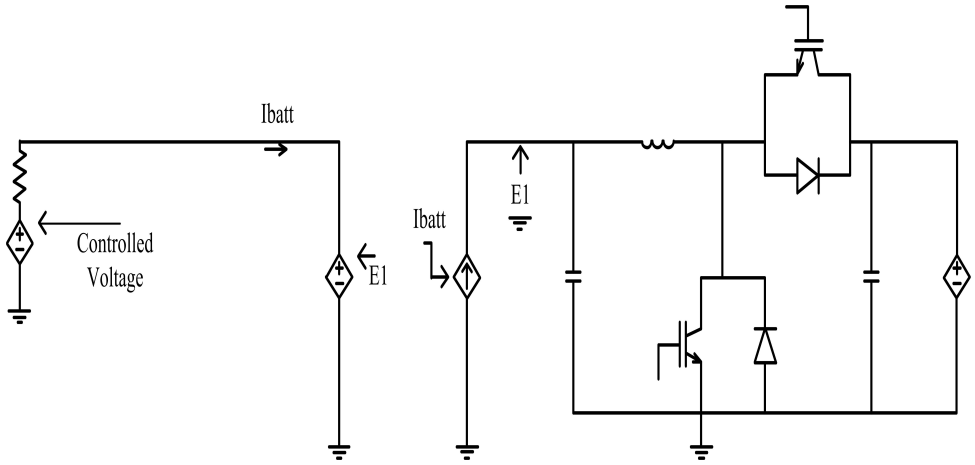

Fig. 3.8: Battery model connected to DC-DC converter .

Figure 3.8 shows a bidirectional DC-DC converter connected to the Shepherd battery model. On the right hand side of the figure the DC-DC converter is shown. The left hand side presents a variable voltage source in series with a resistance. This is a presentation of the Shepherd model. Shepherd model is discussed in previous chapter of this thesis. Connection methodology of these devices in Figure 3.8 is the basis of HIL simulation of batteries. E1 is sensed and is applied to battery. As a feedback, battery current is sensed and is applied to DC-DC converter. In HIL simulation of batteries, the battery model is replaced by a real battery. In this case the applied voltage to the battery is different by a scaling factor from E1; it is called scaled HIL. This will be discussed further in the next chapter.

Sizing methods of components in a DC-DC converter is thoroughly discussed in [51]. By increasing values of inductor and capacitor less ripple will be sensed in the output of the converter.

3.4 Voltage Source Converter (VSC)

A VSC is required to connect an energy storage device with DC power to an AC grid. A VSC changes DC form of the input to AC form in output. Generally speaking the role of a VSC is to create controlled AC voltage. A single-phase VSC is depicted in Figure 3.9. It has two controlled switches and a DC link. Each switch is complement of the other one. For example when S1 is on, S2 is off and vice versa. Consequently the output is either connected to the positive or the negative pole of the DC link. This makes a square wave form in the output. Once applied to a load, depending on the load current will lead or lag the voltage. In Figure 3.10 it is assumed that the VSC cell is connected to an RL load. It shows the waveform of the current and the voltage of the load. This square wave form is composed of many harmonic components. With proper switching algorithm a large fundamental component dominates the rest of harmonics. This means that if Fourier transform of the output is considered, its fundamental mode has high magnitude in comparison to other harmonics. The fundamental frequency behavior of voltage and current in VSC is discussed in [51].

A 3-phase VSC is composed of 6 switches and a capacitor, which is installed on its DC link. Two switches are placed on each phase. Consequently each phase might be connected to the positive or negative of DC link. The DC capacitor is used to stablize the voltage on the DC link. Firing pulses play the most important role in controlling the VSC. There are many methods to control a VSC and to generate

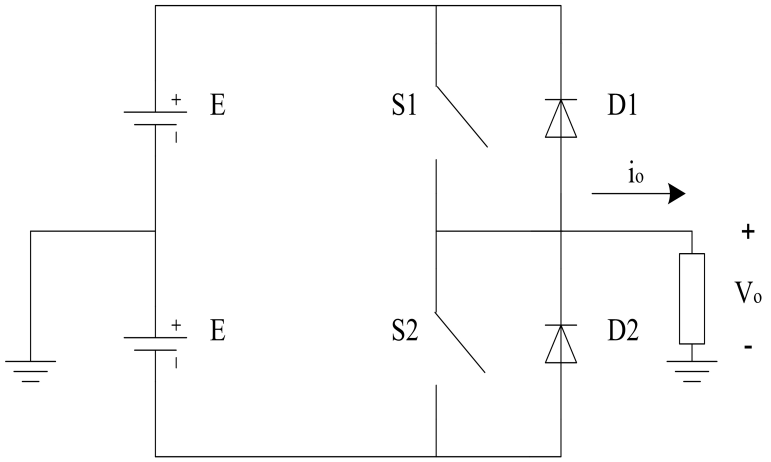

Fig. 3.9: A single phase VSC.

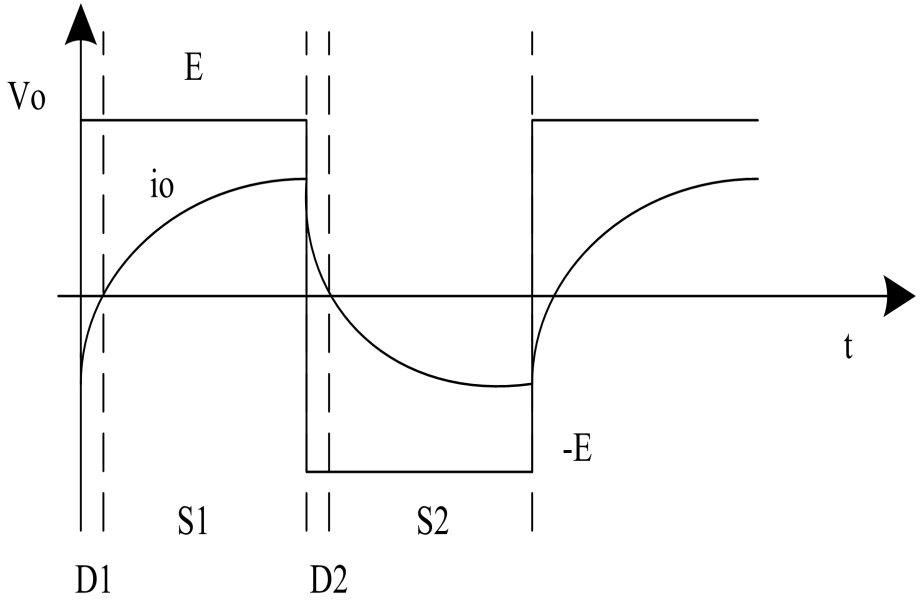

Fig. 3.10: Output waveform of a single phase VSC.

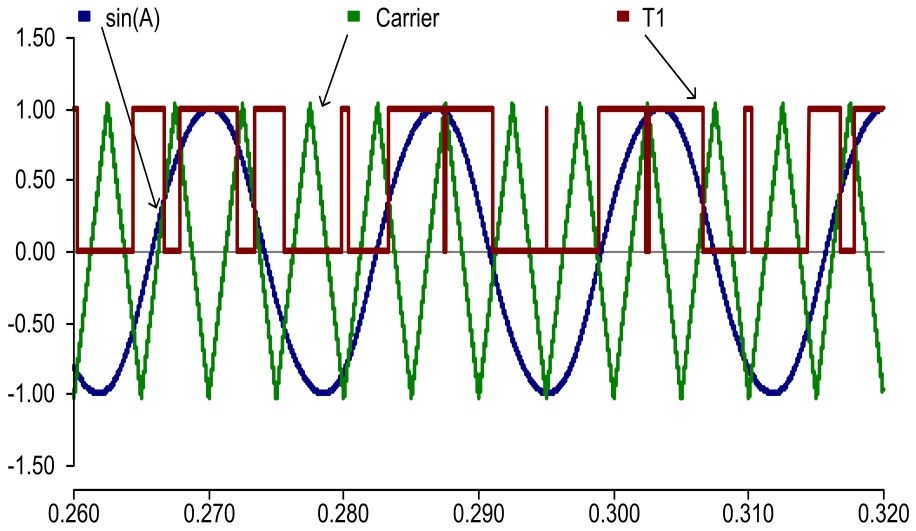

Fig. 3.11: PWM technique.

proper firing signals. The pulse-width-modulation (PWM) technique is used for the purpose of control of switches in the case study of this thesis. To generate firing pulses a sinusoidal reference wave is compared with a triangular carrier wave-form. Whenever the sine wave is larger in amplitude than the triangular wave firing pulse would be one. Whenever it is less in amplitude than triangular wave firing pulse is zero. This leads to a dominant sine wave with the same frequency of carrier in output. Switching frequency is defined by switching frequency of carrier. Figure 3.11 shows this technique.

A phase lock loop (PLL) is used as the reference point for the sine wave. A PLL is an electronic module that locks to the phase of the output. A PLL is a feedback system that detects the phase error and then adjusts the phase of its output.

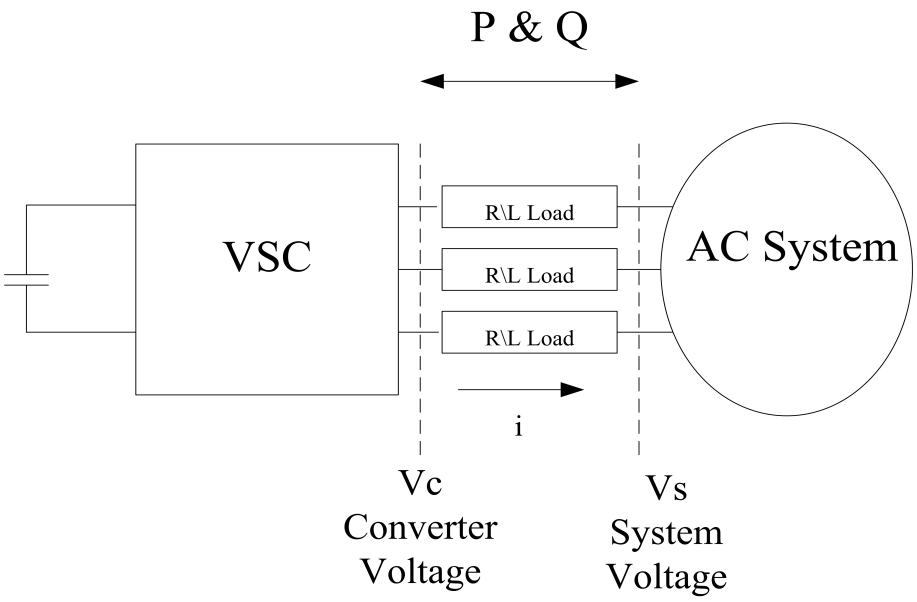

Fig. 3.12: Schematic of VSC connection to grid.

In a three phase VSC, firing pulse are shifted 120 degrees. Phase and magnitude of sine wave which is compared to the triangular wave are important in determining amount of active and reactive power transmitted to the grid.

Vector control method is used to define phase angle and magnitude of the reference sine wave. Figure 3.12 shows the schematic diagram of how a VSC is connected to the grid. Equation (3.9) shows relation between circuit elements in Fig 3.12. Equations (3.10 3.11 3.12) describe parameters that are used in equation (3.9).

$$V_c(t) = L\frac{di}{dt} + Ri + V_s(t) \tag{3.9}$$

$$V_c(t) = [\,V_{ca}(t),\, V_{cb}(t),\, V_{cb}(t)]^T \tag{3.10}$$

$$i_(t) = [i_a(t), i_b(t), i_c(t)]^T \tag{3.11}$$

$$V_s(t) = [\,V_{sa}(t),\, V_{sb}(t),\, V_{sc}(t)]^T \tag{3.12}$$

DQ transform or what is called Park transformation is presented in equation (3.13) and (3.14). Equation (3.9) is changed to equation (3.15,3.16) after using Park transformation. If voltage of source is assumed in form of equations (3.17,3.18,3.19) it can be proved that $V_{sq} = V_m$ and also $V_{sd} = 0$.

$$\boldsymbol{x}_{qd0} = K\boldsymbol{x}_{abc} \tag{3.13}$$

$$K = \frac{2}{3}\begin{bmatrix} \cos\theta & \cos\theta - \frac{2\pi}{3} & \cos\theta + \frac{2\pi}{3} \\ \sin\theta & \sin\theta - \frac{2\pi}{3} & \sin\theta + \frac{2\pi}{3} \\ \frac{1}{2} & \frac{1}{2} & \frac{1}{2} \end{bmatrix} \tag{3.14}$$

$$V_{cq} = r i_q + \omega L i_d + \frac{d i_q}{dt} + V_{sq} \tag{3.15}$$

$$V_{cd} = r i_d - \omega L i_q + \frac{d i_d}{dt} + V_{sd} \tag{3.16}$$

$$V_{sa}(t) = V_m \cos \omega t \tag{3.17}$$

$$V_{sb}(t) = V_m \cos(\omega t - \frac{2\pi}{3}) \tag{3.18}$$

$$V_{sc}(t) = V_m \cos(\omega t + \frac{2\pi}{3}) \tag{3.19}$$

$$P = \frac{3}{2} V_m i_q \tag{3.20}$$

$$Q = \frac{3}{2} V_m i_d \tag{3.21}$$

Figure 3.13 shows DQ control diagram of a VSC. Normally a PI controller is used as the controller in this configuration. By applying inverse Park transformation to the calculated V_{cq} and V_{cd}, the values of the phase and magnitude of the control signal for a PWM method can be defined. By using this method values of transferred active and reactive power can be independently controlled through equations (3.20) and (3.21). Figure 3.14 shows how the simulated VSC in the case

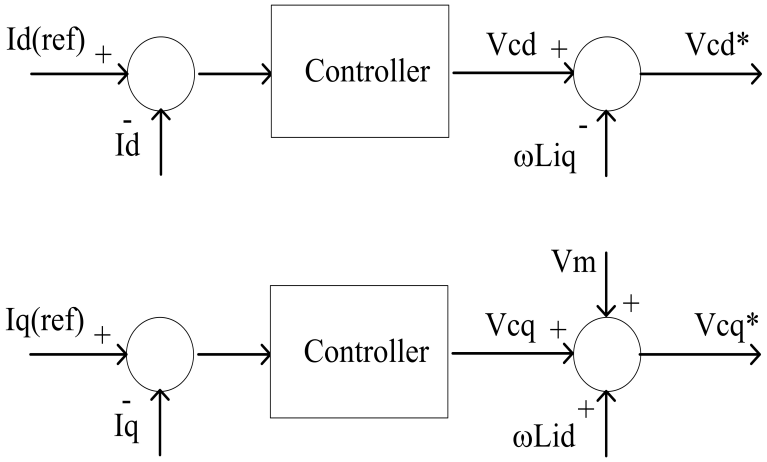

Fig. 3.13: DQ Control diagram of a VSC.

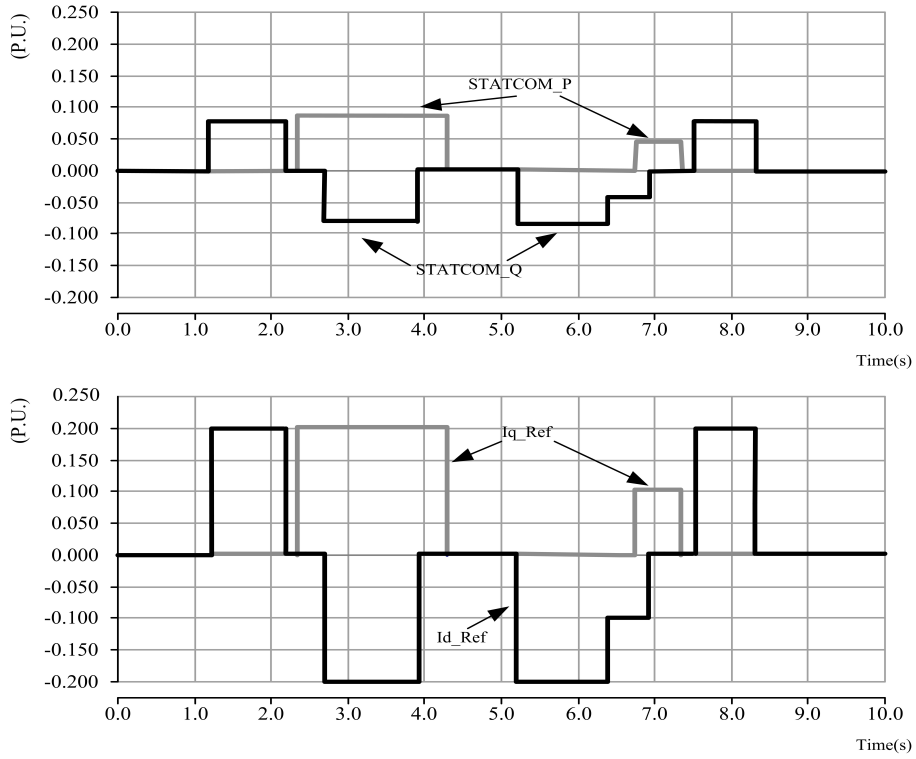

Fig. 3.14: VSC simulation results.

study of this thesis controls active and reactive power independently. An average model is used prior to development of a full converter model to test the control strategy.

In this chapter necessity of using BESS in wind farms was discussed. DC-DC converters and VSC were introduced as part of the required power electronics to connect BESS to wind farms. Vector control method used in the control of VSC was discussed. Finally in Figure 3.14 simulation results of VSC in PSCAD environment were shown.

4. EXPERIMENTS

In this chapter HIL simulation results of a type 1 wind farm will be investigated. To perform an HIL simulation it is recommended to do a software simulation at first. It is easier to tune controllers and to perform component sizing in a fully software-based simulation. HIL simulation is performed on a real-time basis. In addition as one part of simulation has physical existence, implementing HIL simulation without verifying software simulation in advance might not be safe. For example in case of using batteries as the external physical part of an HIL simulation, over-current might happen for the battery as a consequence of improperly tuned PI controllers.

To investigate results of HIL simulation, more details about case study is provided in first subsection. Then software simulation results will be presented. Afterwards HIL setup will be discussed. Then, HIL simulation results will be shown. This chapter ends with the description of a method to measure battery efficiency in HIL simulation.

4.1 Description of a Type 1 Wind Farm

Figure 4.1 depicts the schematic diagram of the case study. A wind speed profile is the input to a wind turbine. It also requires generated power of generator as a feedback signal to adjust pitch angle of the blades. Mechanical torque on the generator shaft is the output of this block. In this case study a 1.32 MW SCIG is used as generator. It starts up in speed control mode as a motor and then switches to torque control mode and becomes a generator. Line to line voltage of the low voltage side is assumed to be 690V. Boost up transformer increases voltage up to 13.8kV on the high voltage side. The point of common coupling (PCC) is where the induction generator and BESS are connected together. Figure 4.2 shows the schematic diagram of the case study with more details. Vx is the scaled value of the DC link voltage of the VSC. Ix is also the scaled value of current of variable voltage source in the DC-DC converter. This helps to implement the scaled HIL configuration appropriately.

The generated power from wind is measured and is compared to the expected generated power. BESS is used to regulate generated power. Figure 4.3 shows the control diagram of the system. Once the VSC absorbs active power from grid, the voltage of the DC link increases. To decrease DC link voltage DC-DC converter charges batteries. On the other hand, once VSC exports active power to grid voltage of the DC link decreases. To increase the voltage of the DC link batteries are discharged. Battery charge or discharge reference current

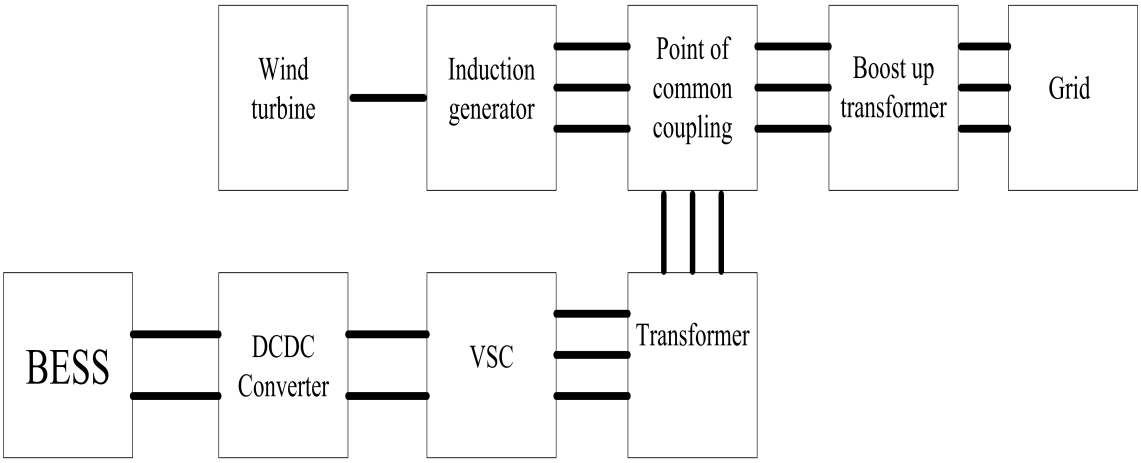

Fig. 4.1: Schematic diagram of simulated case study.

is limited in the deployed control strategy to prevent over-current of batteries. There have been some studies over different control strategies in application of BESS in wind farms [8, 52, 53]. In [53] it is recommended to keep the battery SoC between 30-70 percent during normal operation. This will increase battery life cycle. Since the maximum capacity of BESS is not used, battery storage with higher capacity should be used. To harvest maximum energy, it is suggested to charge batteries with highest possible current. On the other hand at the time of discharge, batteries are discharged at highest possible discharge rate. This is the best charge or discharge strategy in this application as charging or discharging periods are not defined. This means that it is better to charge batteries as fast as possible because the length of charging period cannot be predicted as a result of uncertainly in the wind speed.

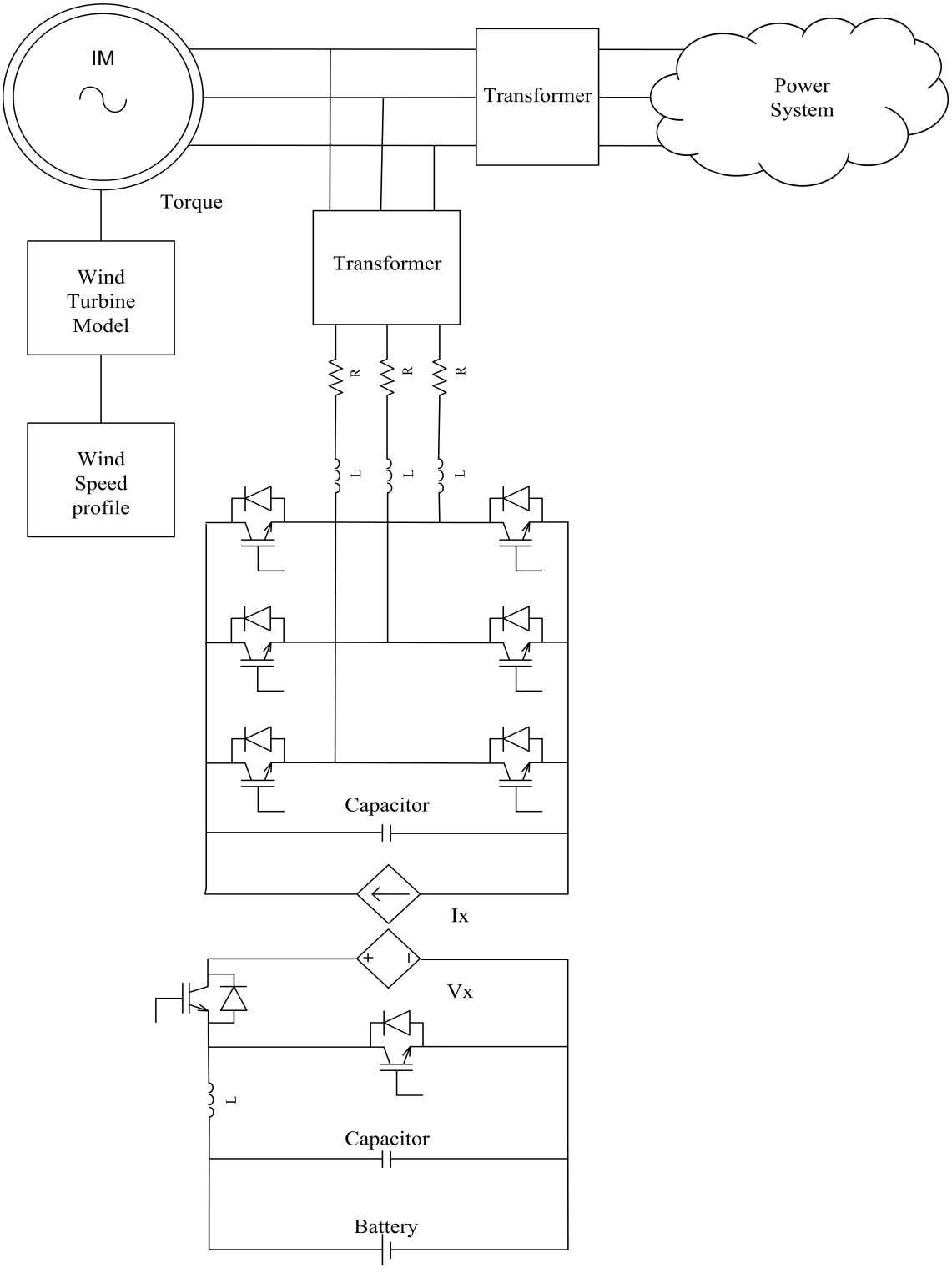

Fig. 4.2: Schematic diagram of case study.

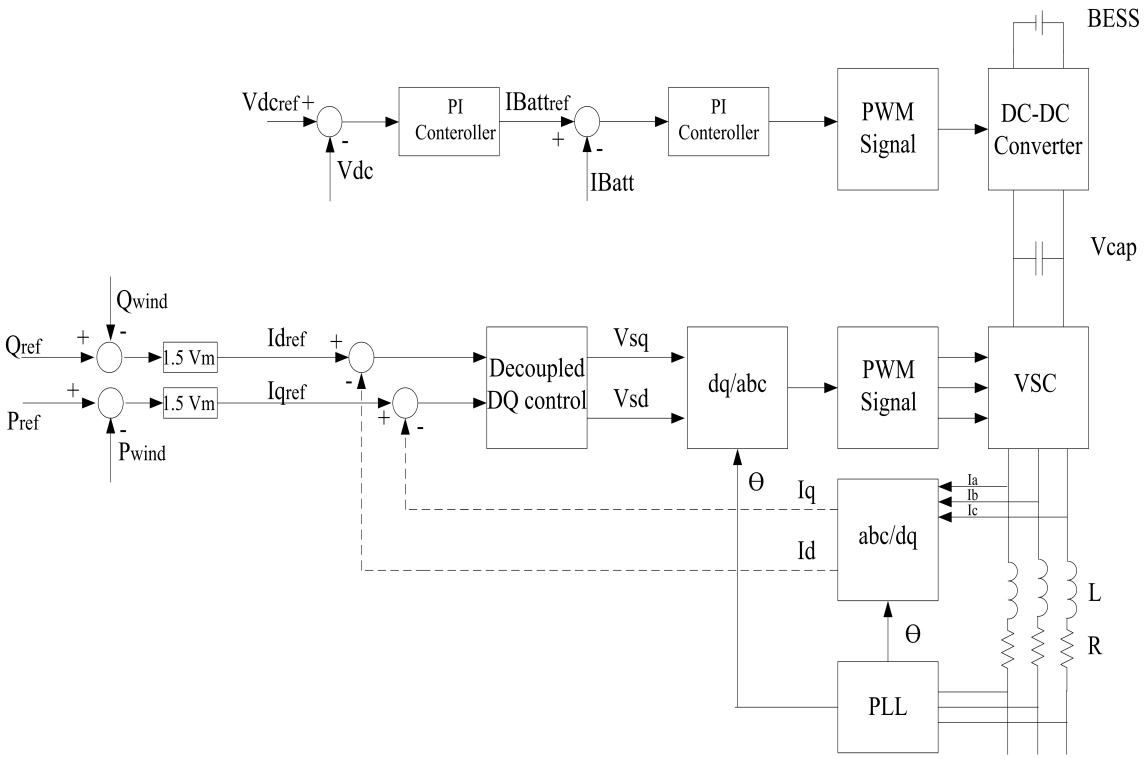

Fig. 4.3: Control schematic of case study.

4.1.1 PSCAD Simulation Results

PSCAD/EMTDC is used as the simulation environment. PSCAD/EMTDC is a fast and accurate power system simulation software for the design and verification of all types of power systems. BESS, wind turbine, generator, DC-DC converter and VSC are simulated in PSCAD/EMTDC. It is important to note that even a large size BESS is not able to eliminate the power deviations completely. Figure 4.4 shows wind speed variation in PSCAD/EMTDC simulation of case study. Wind gust has a peak velocity of 1 $\frac{m}{s}$ in this wind profile. Pitch control system tries to control effect of wind speed variation by changing pitch angle. This is depicted in Figure 4.5. As it was previously mentioned pitch control is not able to fully cancel the effect of wind speed variations. Consequently, produced power of wind turbine changes. Figure 4.6 shows the produced wind power, the exported power from wind farm and the contribution of BESS. The produced wind power changes as a result of wind speed variation. The exported power is more or less constant as BESS has compensated the effect of wind variation. The expected dispatched power is less than the produced power in Figure 4.6, consequently it is expected that BESS should absorb extra power. Figure 4.7 shows the current of one cell of BESS. In the transient period the battery cells are discharged to charge capacitors on DC link although it is charged for most of the simulation time.

As previously mentioned, the control strategy tries to regulate the DC link voltage. Figure 4.8 shows the DC link voltage. At first DC capacitors, which are

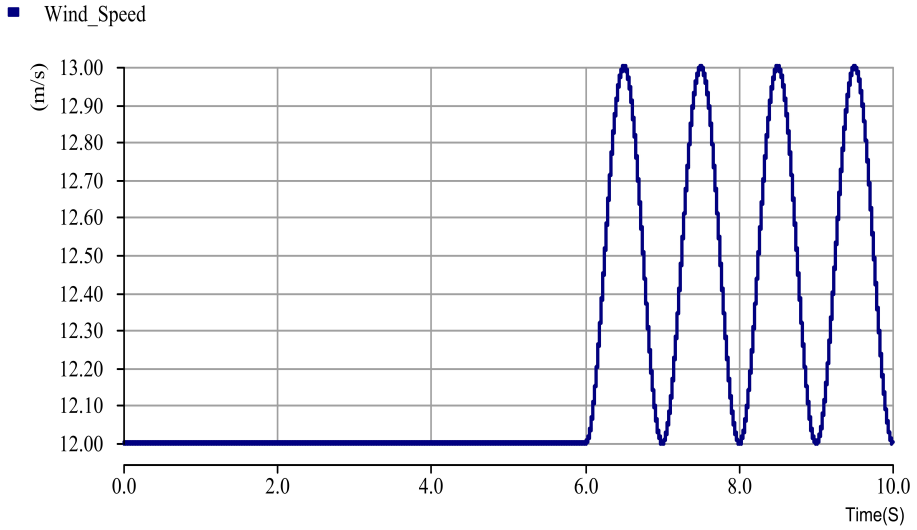

Fig. 4.4: Wind speed variations.

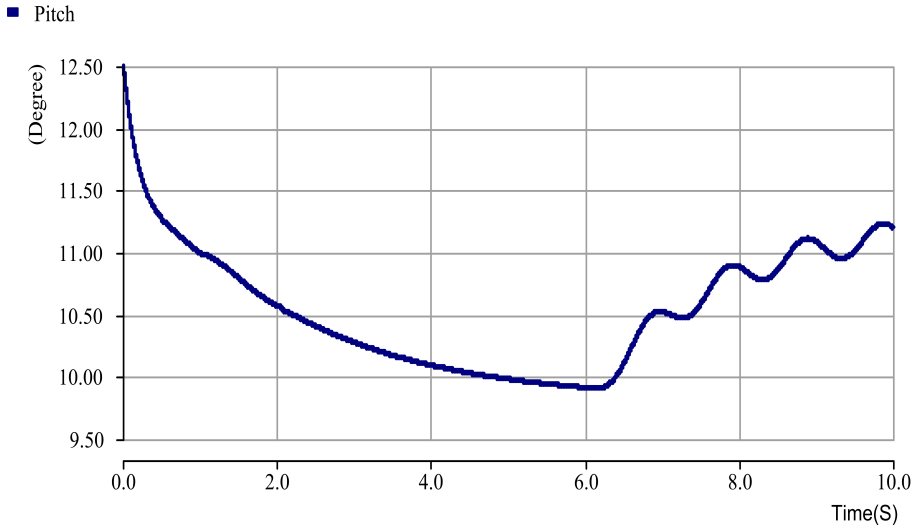

Fig. 4.5: Pitch angle variations.

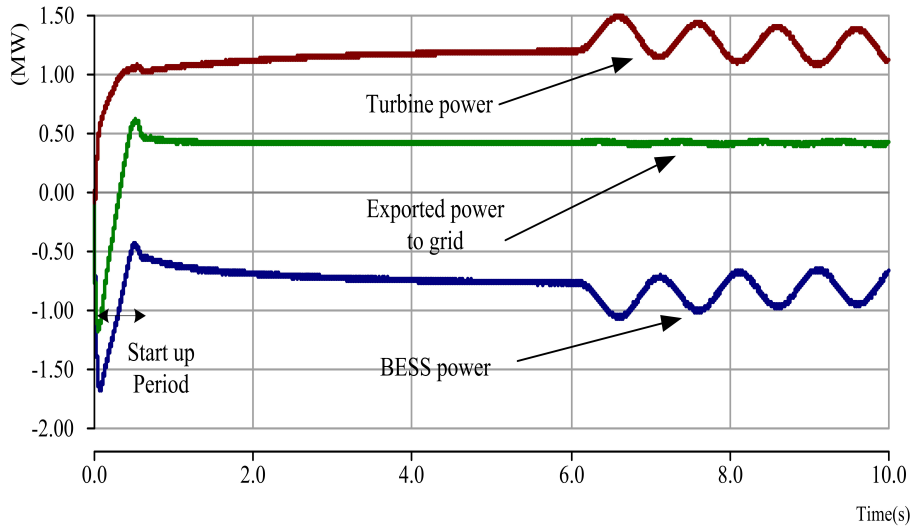

Fig. 4.6: Produced wind power, exported power from wind farm and contribution of BESS .

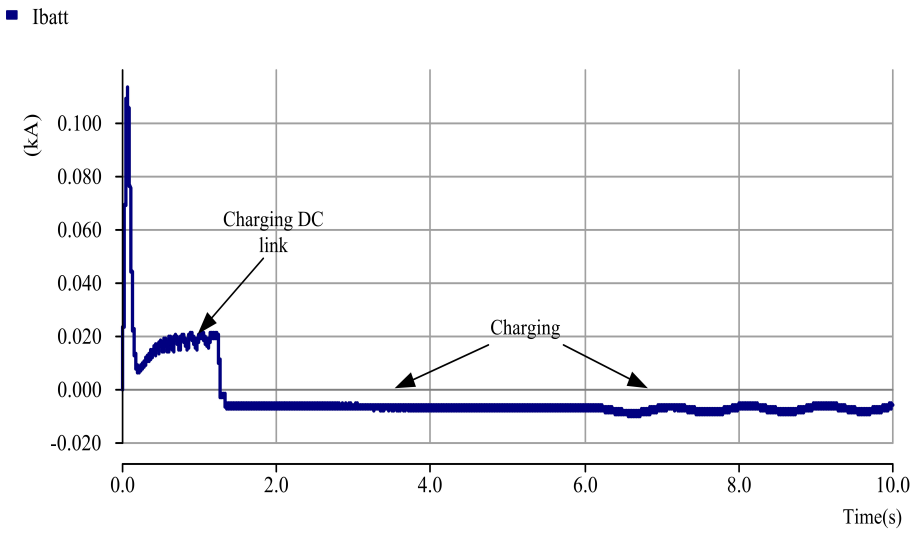

Fig. 4.7: Battery current profile.

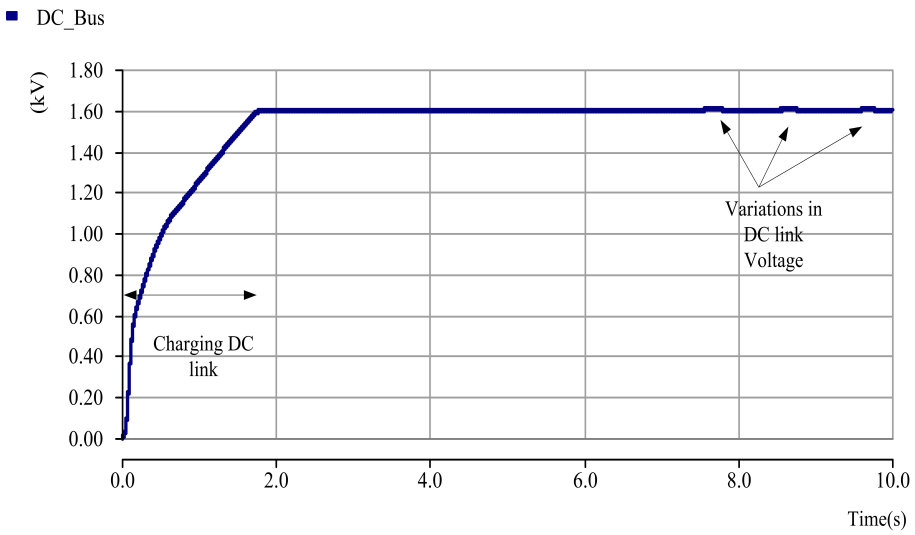

Fig. 4.8: DC link voltage.

installed on the DC link need to be charged. This is a transient period. After capacitors are charged, the DC voltage remains regulated.

Figure 4.9 shows the produced wind power, the exported power from the wind farm and the contribution of BESS. The produced wind power changes as a result of wind speed variations. In Figure 4.9 the dispatched power is the same as the rated power of wind turbine at wind speed of 12 $\frac{m}{s}$. Once wind speed increases BESS needs to be charged. When wind speed decreases BESS is discharged. Figure 4.10 shows current profile of a battery cell which is used in the simulation.

Figure 4.11 shows the produced wind power, the exported power from wind farm and the contribution of BESS. Produced wind power changes as a result of wind speed variation. When wind power is less than the dispatched power it is expected that the BESS is discharged. Figure 4.12 shows current profile of a

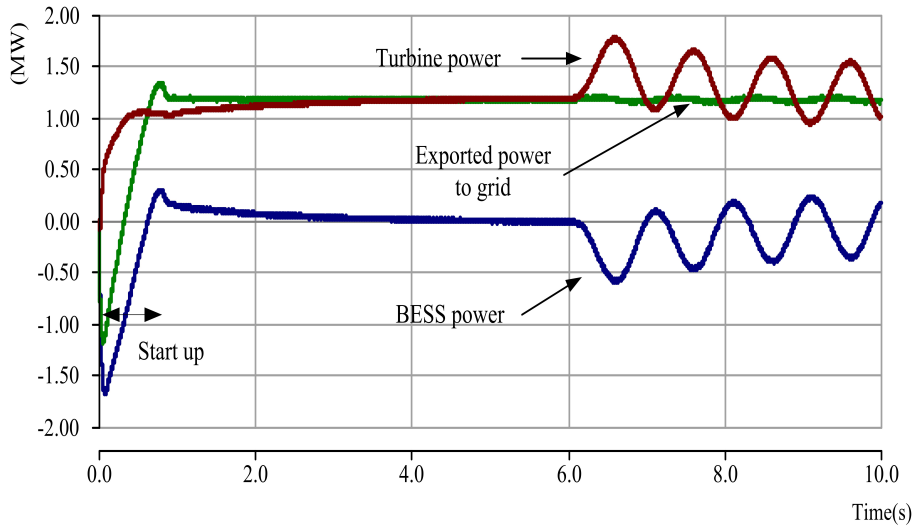

Fig. 4.9: Produced wind power, exported power from wind farm and contribution of BESS.

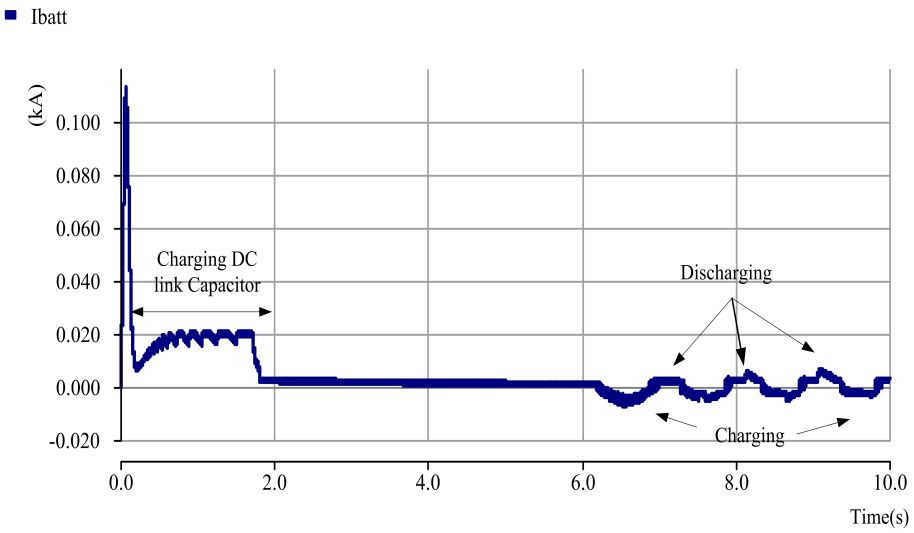

Fig. 4.10: Battery current profile.

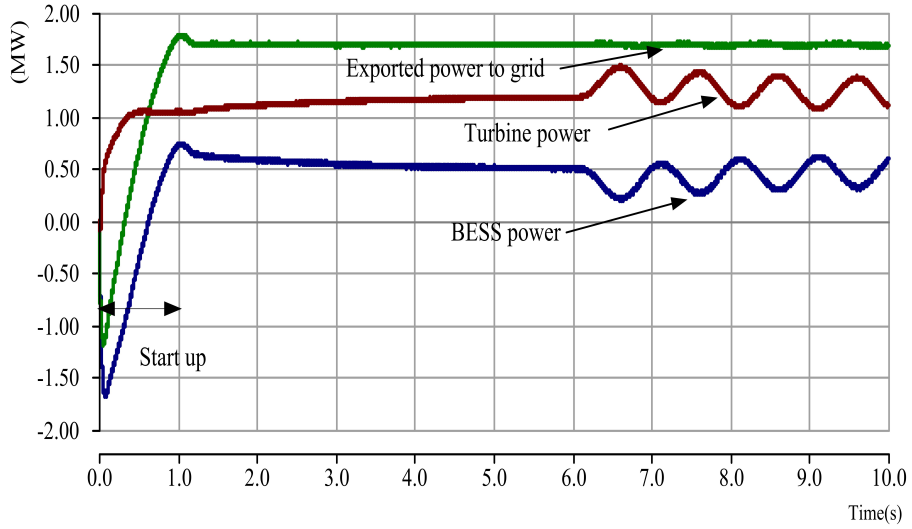

Fig. 4.11: Produced wind power, exported power from wind farm and contribution of BESS.

battery cell which is used in the simulation.

4.2 HIL Setup

Figure 4.13 shows devices that are involved in an HIL simulation. This configuration of HIL is composed of an RTDS as the real-time simulator, I/O cards and an amplifier, which are interface devices, and also batteries. As it is shown RTDS is used as simulation environment to simulate the wind farm, the grid, the transformers, the DC-DC converter and the VSC.

RTDS is a digital simulator used to perform HIL testing of physical devices, such as protection equipment and control equipment used in power systems. HIL testing is a method to test physical devices. In an HIL testing system signals

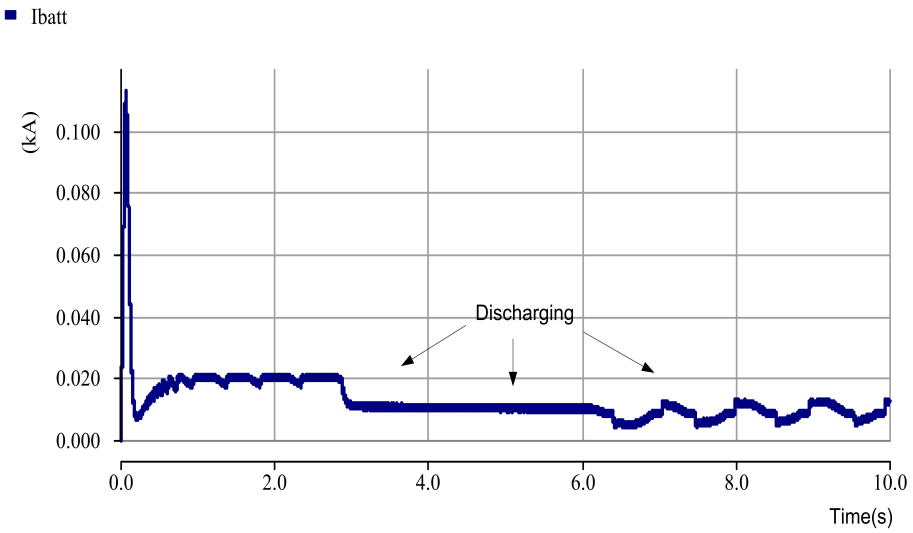

Fig. 4.12: Battery current profile.

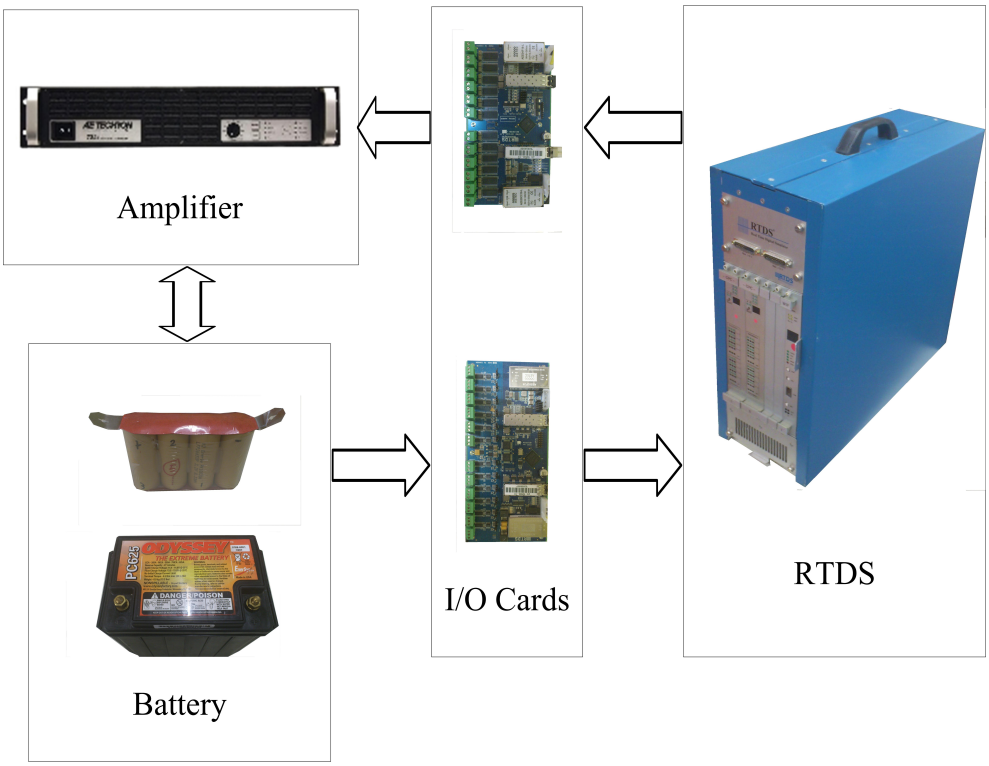

Fig. 4.13: HIL schematic.

are taken out from the simulation, and are provided to control the devices that are under test. The output from the device being tested is then fed back into the simulation. It might require exchange of input and output signals to control the process and acquire required data. RTDS is a combination of hardware and software. Power network models are created in the RSCAD interface software. RSCAD provides a large number of electrical components from model libraries. RSCAD is an interface with the RTDS Simulator hardware.

AE Techron 7224 amplifier is used to charge/discharge batteries with the same pattern as required. It is a 1 kVA amplifier. It can support DC terminal to 300 kHz bandwidth. This amplifier provides 40 msec pulse with up to 52 Amperes peak current. In continuous mode, a 7224 amplifier can provide 1,100 Watts of output power. Up to four amplifiers can be combined in series or parallel to provide higher power ratings. It can be used in either voltage or current mode.

The I/O cards are optically isolated. The analog-out card has a total of 12 outputs. It can refresh data at 1.0μS intervals. Analog-in card can update data at minimum rate of 6μS intervals. The analog input/output can range between a maximum of 10 Vpeak.

A Hall effect sensor is used to measure the current. Figure 4.14 shows the Hall effect module used in this setup. An external ammeter is frequently used to calibrate the Hall effect module.

To provide more protection for the batteries, a 10 ampere fuse has been used

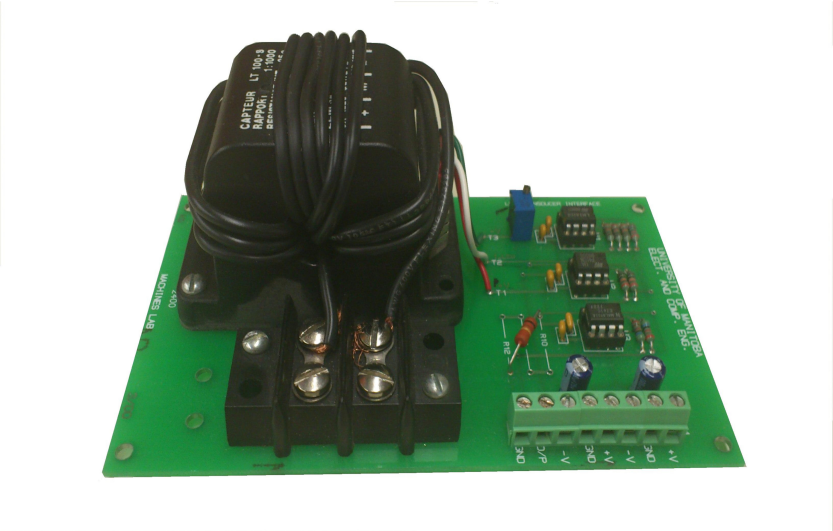

Fig. 4.14: Hall effect sensor used.

in series with the batteries. This will provide extra protection for batteries in abnormal operating situations.

4.2.1 HIL Simulation Results

As it was previously discussed an HIL test needs a simulation structure. RTDS is used as simulation environment. It enables real-time interaction of batteries with the simulation environment. RSCAD is the software interface to work with RTDS. Many devices are available in the RSCAD library with which a system can be presented. Figure 4.15 depicts the runtime environment of RSCAD software. This is the graphic interface, which enables users to monitor values and change simulation parameters. As depicted in Figure 4.15 battery voltage, battery current, SoC, DC link voltage and values of active and reactive power of wind turbine, BESS

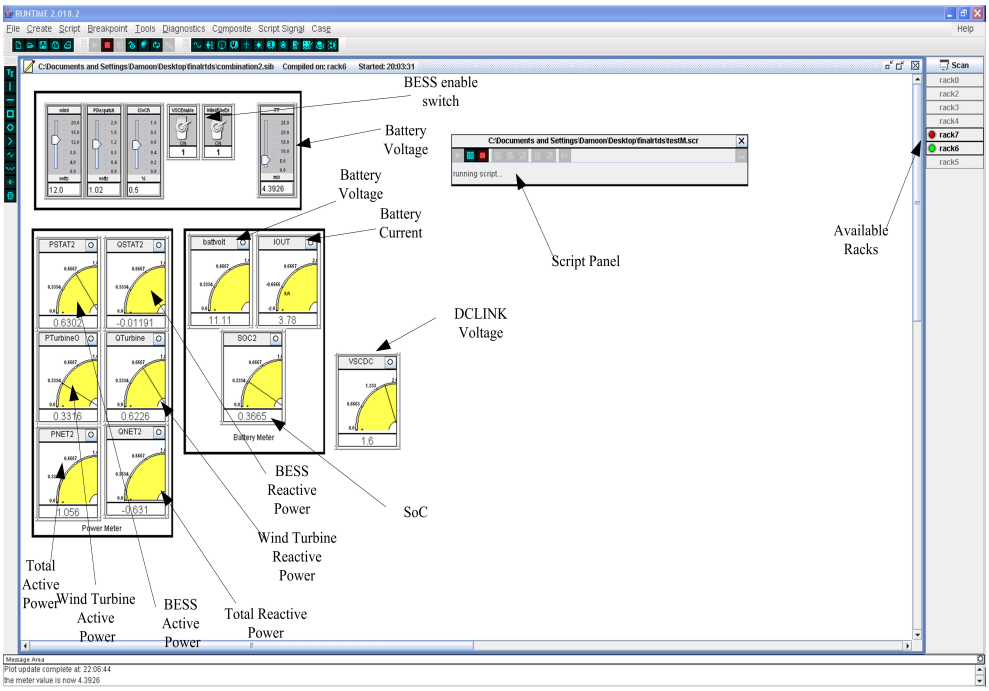

Fig. 4.15: Runtime environment in RSCAD.

and wind farm are monitored. Wind profile is read from a text file and is used as the input to the wind turbine using a script. The scripts enable RTDS to do certain tasks at specific times. For example the value of voltage can be acquired every second and saved in an output file.

Variation of wind speed changes the produced active power in wind turbine. Figure 4.16 shows variation in wind power. BESS is used to reduce the power variation in the output of the wind farm. The aim is to set the output power at 1MW.

Figure 4.17 shows exported power to grid in simulation environment. The effect of wind speed variations is reduced and power is maintained around 1MW.

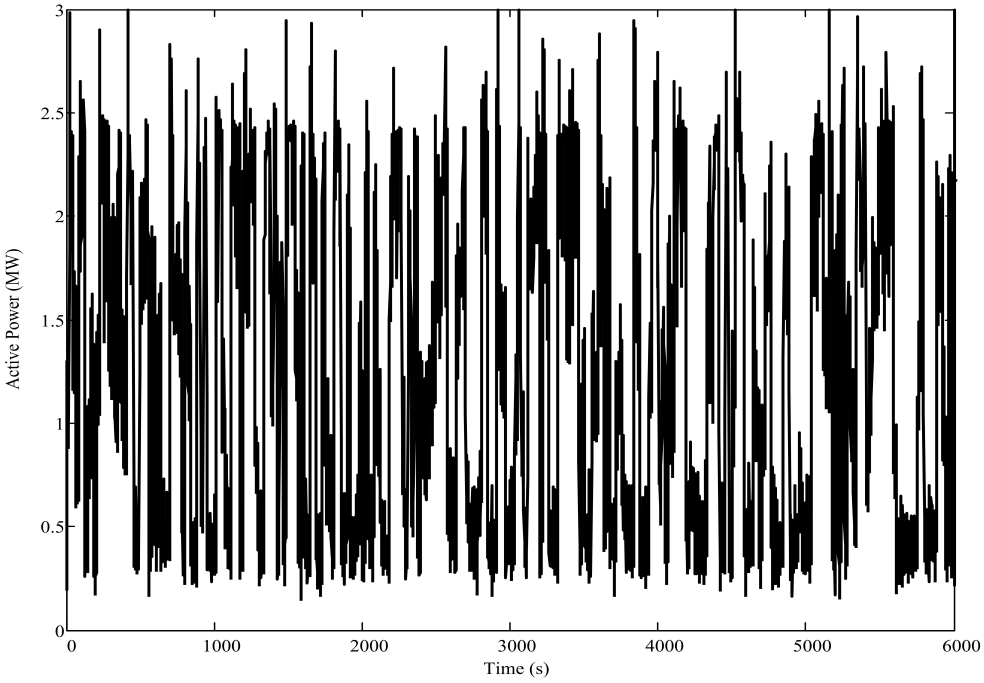

Fig. 4.16: Produced active power of wind turbine.

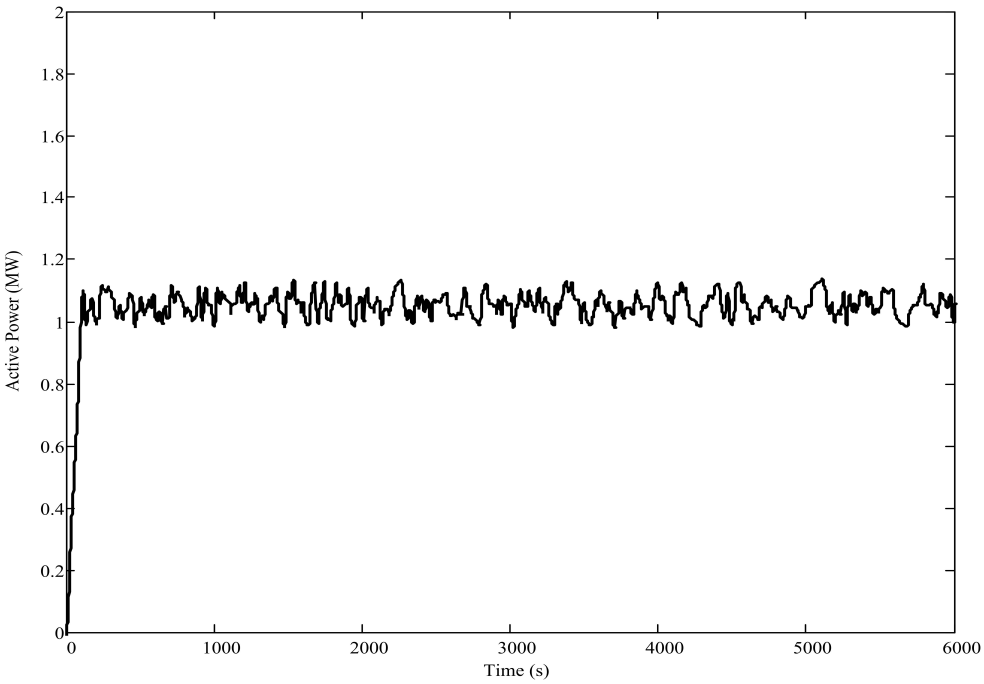

Fig. 4.17: Exported active power to grid.

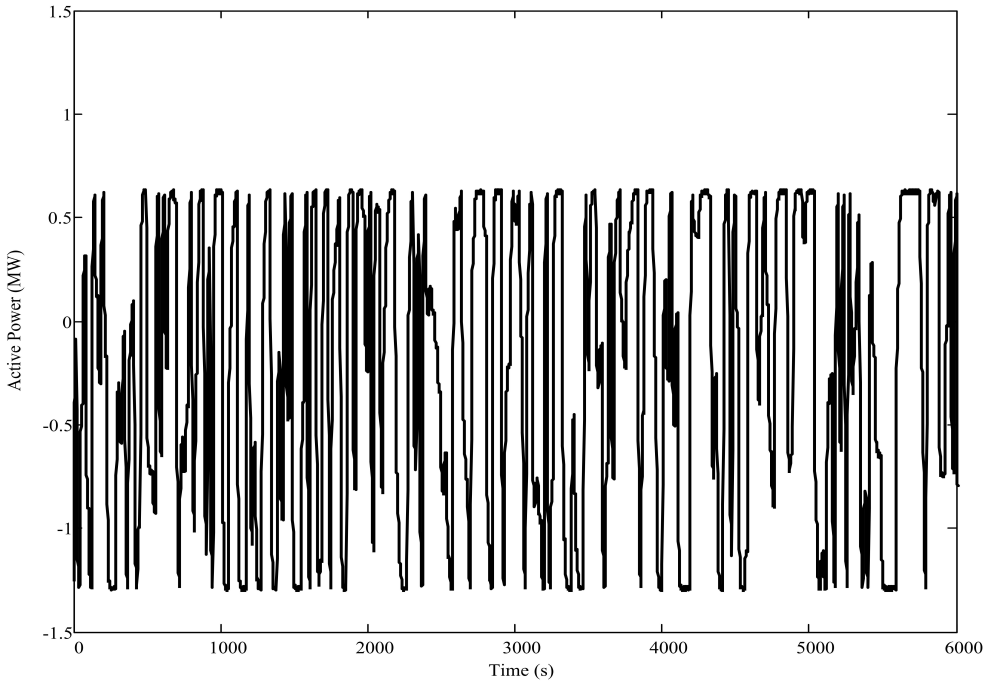

Fig. 4.18: BESS power profile.

BESS is used to reduce variations of produced power. Figure 4.18 shows change in BESS power. BESS is used to keep DC link voltage of VSC constant. Figure 4.19 shows DC link voltage.

Figure 4.20 shows the current profile of the 18Ah Odyssey lead-acid battery. It is important to notice once more that this is a reduced HIL simulation. This means that the voltage of battery is multiplied by 32. Battery current is also multiplied by 800. Scaled values of voltage and current are used in simulation. This resembles a BESS composed of 32×800 batteries.

The average voltage of the battery drops during simulation. This is depicted in Figure 4.21. Battery SoC is depicted in Figure 4.22. SoC of battery also

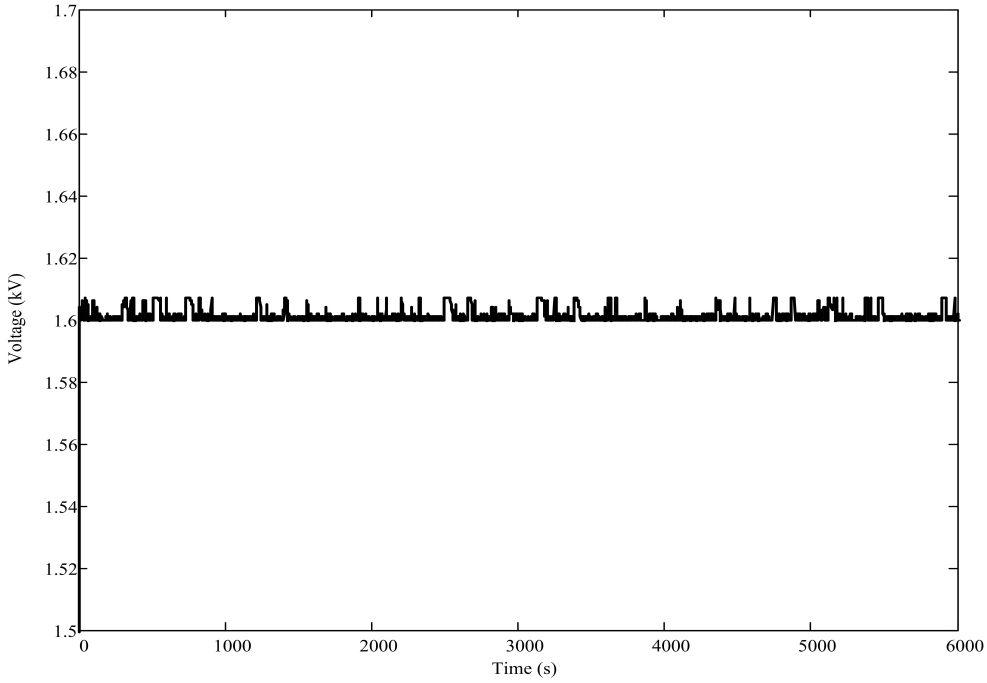

Fig. 4.19: DC link voltage.

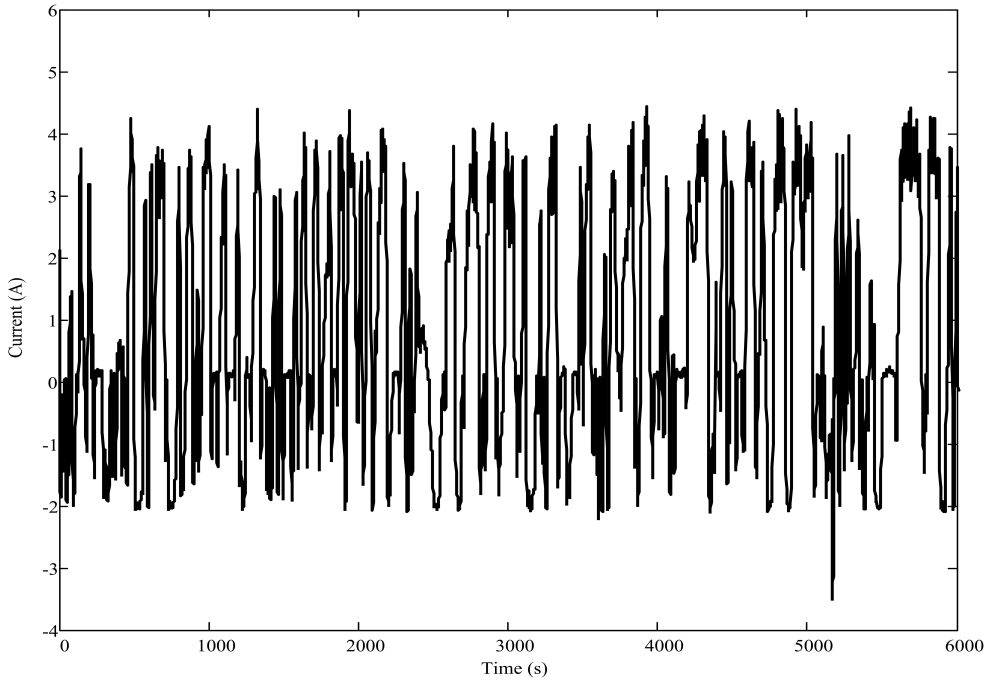

Fig. 4.20: Battery current profile.

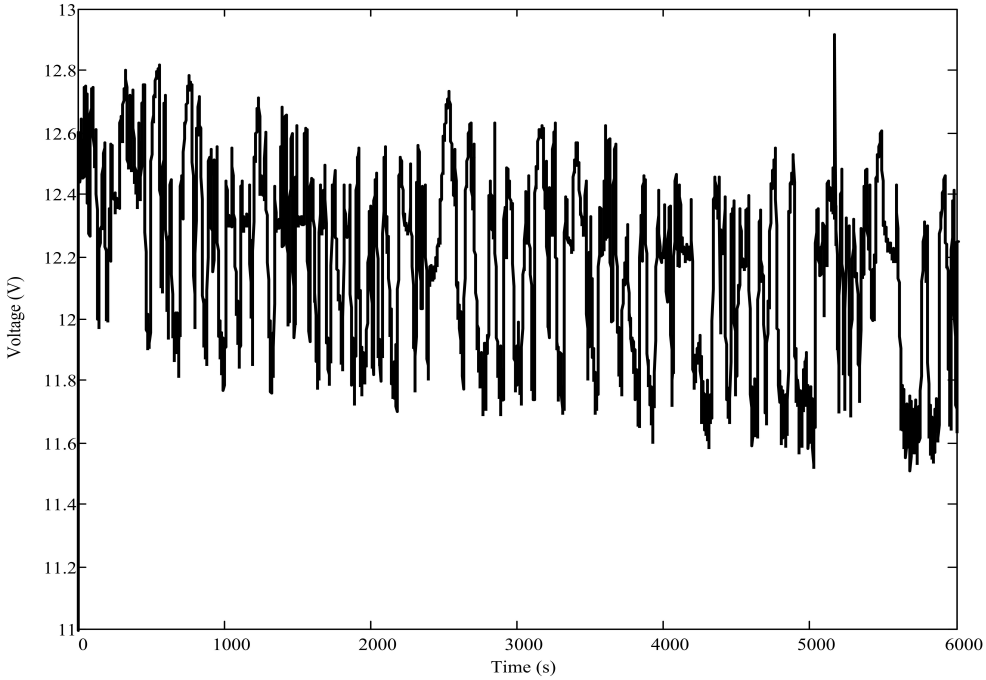

Fig. 4.21: Battery voltage profile.

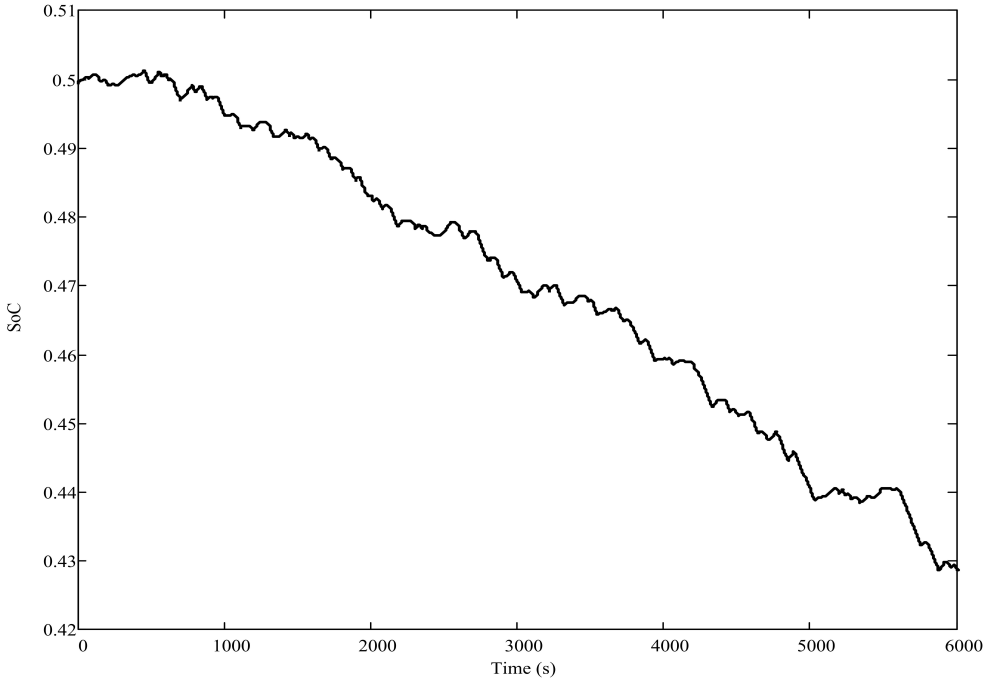

Fig. 4.22: Battery SoC.

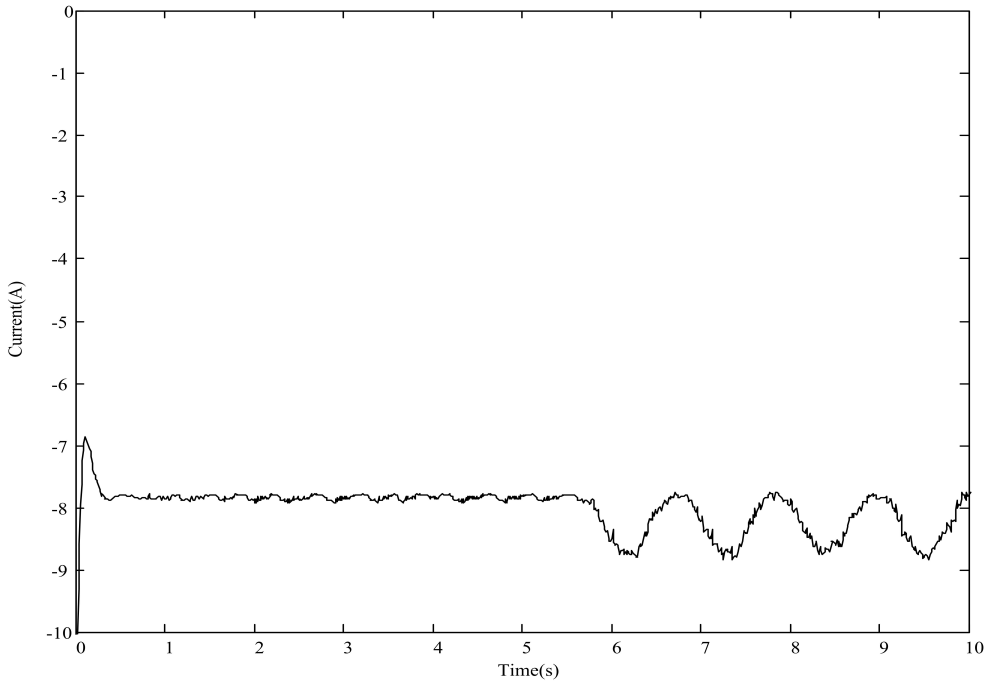

Fig. 4.23: Battery current change with a typical wind gust.

reduces during simulation. This shows that during HIL simulation battery is more discharged than it is charged. It is obvious that different wind profiles have different effect on BESS. For example Figure 4.23 shows effect of HIL on the tested battery with the same wind profile of Figure 4.4. This current waveform is essentially similar to the one shown in Figure 4.12. Depending on wind profile and expected output power of wind farm batteries in BESS might be charged or discharged. Depth of discharge of batteries, charge or discharge rates and also voltage and current profile of batteries are unique for different wind profiles.

4.2.2 Using HIL for Efficiency Measurement

To measure efficiency of a battery in HIL simulation, a battery with a certain SoC is installed in HIL setup. During HIL simulation battery is either charged or discharged according to system requirements. SoC of battery is traced by coulomb counting method with the assumption that η=1. This false assumption causes error in calculation of SoC. At the end of HIL simulation the SoC of the battery is measured by discharging it. This is assumed to be the actual SoC of the battery. Once the battery is discharged, its voltage drops. Battery is considered fully depleted once its voltage drops below a certain voltage. This voltage is usually indicated by the manufacturer. Difference of measured and actual SoC determines battery efficiency. In Figure 4.22 the SoC of battery at the end of HIL simulation is depicted. At the end of simulation the actual SoC is measured once more by discharging battery. The discharge method shows that the actual battery SoC is 31 percent. it is assumed that efficiency of battery equals to 1 at the time of discharge. In this way average efficiency of battery at the time of charging is $\frac{31}{43}$ for PC625 Odyssey lead-acid battery in HIL simulation of type 1 wind farm. Once $\frac{31}{43}$ is used as battery efficiency at charging time and unity is considered as battery efficiency at discharge time, final calculated SoC would be same as the actual battery SoC(0.31). Efficiency of LFP2650P lithium ion battery is measured to be 98 percent. More investigations shows that when wind profile is smoother (which means that batteries are less charged and discharged), battery efficiency

for lead acid battery increases slightly. In addition to discussed method that gives an estimation of efficiency, equation (2.5) can be used to measure exact value of efficiency.

In this chapter case study of this thesis was described in details. Simulation results of the PSCAD environment were shown. Afterwards HIL simulation results were presented. Then, the method which was used to measure battery efficiency in HIL simulation was discussed. This method can be used to measure battery efficiency in different applications. Finally, battery efficiencies for lead-acid and lithium-ion battteries were measured.

5. CONCLUSIONS, CONTRIBUTIONS AND FUTURE DIRECTIONS

At the first stage of this thesis important characteristics of a battery that are important for system level design were studied. Thevenin, Randle and Shepherd models were developed for PC625 Odyssey lead-acid and LFP2650P lithium ion batteries. Then a battery model, a bidirectional DC-DC converter and a voltage source converter were implemented in PSCAD-EMTDC software. A wind farm was implemented in PSCAD-EMTDC with the aim of reducing power variations caused by the change of wind speed. Batteries were used to reduce these variations. Then HIL simulation was used to alleviate the need for a battery model. The aim of this chapter is to highlight important findings of this thesis and state directions along with this work can be extended.

5.1 Contributions

The main conclusions and contributions of this research are highlighted as follows:

1. Study of battery parameters: Important battery parameters used in system

level design were studied thoroughly. Many charge/discharge curves were extracted for battery types used in this study. Investigations showed that the open circuit voltage after rest time can be used to estimate the SoC of batteries. Coulomb counting method, which is one of the most popular methods to estimate SoC, was used in this study.

2. Development of battery models: Different battery models were discussed. Battery models for PC625 Odyssey lead-acid battery and also LFP2650P lithium ion battery were developed. Shepherd model was chosen to be used in the PSCAD/EMTDC environment. Comparison of battery models showed that Shepherd model provides more accurate results in a wider range of SoC variations. In Shepherd model voltage of source changes with change in SoC while in other models which are studied here voltage of source remains constant.

3. Application of HIL battery simulation: HIL simulation was suggested to be used as an alternative to battery models. Although battery models might be accurate for some applications or some portion of the operating range, as battery characteristics change over time, after certain time these models become inaccurate. Internal resistance of battery and capacity of battery change by time. This is recognized as the aging effect in battery. Aging is a function of depth of discharge, and history of usage of the battery. HIL

simulation provides an opportunity for using a physical battery instead of battery models. This provides the user with more accurate results than software simulations that only use battery models. Real time battery simulation is a unique method to investigate battery characteristics under test condition.

4. Development of a Type 1 wind farm model: A type 1 wind farm model was used as case scenario to study the effect of change of the wind speed on BESS used to regulate the output power of wind farm. This case scenario was implemented in HIL configuration. Principles of wind power generation were studied and used in the case study. To connect a battery to grid a DC-DC converter and a VSC should be used. A bi-directional DC-DC converter and also a VSC were implemented as required power electronics of case study in PSCAD and also RSCAD environment. Vector control method was used to control VSC.

5. HIL for battery efficiency measurement: HIL simulation was introduced as a method to measure efficiency of a battery. Efficiency of a battery is an important factor in tracing its SoC if coulomb counting method is used. Efficiency of a battery is affected by different parameters. Charge/discharge rates, SoC, DoD and aging factor change battery efficiency. Battery efficiency of a certain type of battery is different in different applications. For

example in vehicle applications a battery might be charged or discharged more frequently than in a wind farm. This affects the efficiency of a battery. HIL simulation provides the opportunity of studying battery efficiency in a situation, which is close to real operating condition.

5.2 Recommendations for Future Work

A possible extension of this work is to consider the effect of different wind profiles on the efficiency of batteries in HIL configuration. It is possible to study the effect of a certain wind profile, which is for example applied to wind station in a certain place. Different wind profiles might have different effects on BESS. This provides the opportunity of having a better estimation of battery efficiency. Battery efficiency might not be the same for different applications or for different battery types. Accurate battery efficiency leads to a more accurate trace of SoC of battery. SoC of a battery is an important symbol of the amount of energy stored in the battery. Maximum possible energy that can be stored in a battery plays an important role in sizing of a battery storage system. It is recommended to use HIL simulation for a more accurate sizing of battery energy storage in a wind farm. HIL simulation let designers to have more accurate simulation results as a real battery is used. An inaccurate battery model causes an inaccurate sizing of battery energy storage. Since a battery pack is composed of many battery cells and to reduce the effect of inaccuracy of a scaled HIL, It is also suggested to do

the HIL for different battery cells to consider manufacturing variations of different batteries and do a statistical analysis of possible variation in simulation results.

REFERENCES

[1] J. Larminie and J. Lowry, *Electric Vehicle Technology Explained*. John Wiley and Sons, 2003.

[2] K. Divya1 and J. Stergaard, "Battery energy storage technology for power systems an overview," *Journal of Electric Power Systems Research*, no. 79, pp. 511–520, Apr. 2009.

[3] T. Ackermann, *Wind Power in Power Systems*. John Wiley and Sons, 2005.

[4] T. Mostafa, "Wind farms production:control and prediction," Ph.D. dissertation, University of Waterloo, 2007.

[5] P. Keung and Y. Kazachkov, "Generic models of wind turbines for power system stability studies," *8th International Conference on Advances in Power System Control, Operation and Management*, pp. 1–6, 2009.

[6] G. Masters, *Renewable and Efficient Electric Power Systems*. John Wiley and Sons, 2004.

[7] S. Mohod and M. Aware, "A statcom-control scheme for grid connected wind energy system for power quality improvement," *IEEE Systems Journal*, no. 4, pp. 346–352, Sept. 2010.

[8] S. Teleke, L. Anderson, A. Huang, S. Bhattacharya, and S. Atcitty, "Statcom with energy storage for smoothing intermittent wind farm power," *Power and Energy Society General Meeting - Conversion and Delivery of Electrical Energy in the 21st Century*, no. 79, pp. 1 – 6, July 2008.

[9] D. Haifeng, W. Xuezhe, and S. Zechang, "A new soh prediction concept for the power lithium-ion battery used on hevs," *Vehicle Power and Propulsion Conference*, 2009.

[10] K. Divya1 and J. stergaard, "Battery energy storage technology for power systems an overview," *Innovative Technologies for an Efficient and Reliable Electricity Supply*, 2007.

[11] J. Dogger, B. Roossien, and F. Nieuwenhout, "Characterization of li-ion batteries for intelligent management of distributed grid-connected storage," *IEEE Transactions on Energy Conversion*, no. 26, p. 256262, Mar. 2011.

[12] B. Liaw, R. Jungst, G. Nagasubramanian, H. Case, and D. Doughty, "Modeling capacity fade in lithium-ion cells," *Journal of Power Sources*, no. 140, pp. 157–161, Aug. 2005.

[13] M. Broussley, S. Herreyre, P. Biensan, and P. Kasztejna, "Aging mechanism in li ion cells and calender life prediction," *Journal of Power Sources*, no. 140, pp. 13–21, Aug. 2001.

[14] D. Winkler and C. Guhmann, "Hardware-in-the-loop simulation of hybrid electric vehicle using modelica/dymola," *22nd International Battery Hybrid Fuelcell Elec Vehicle Symp. Exhib*, pp. 349 – 356, 2006.

[15] L. Cheng and Z. Lipeng, "Hardware-in-the-loop simulation and its application in electric vehicle development," *Proc. Vehicle power and propulsion conference*, Sept. 2008.

[16] J. Jeon, J. Kim, and H. Kim, "Development of hardware in-the-loop simulation system for testing operation and control function of microgrid," *IEEE transaction on power electronics*, vol. 25, Dec. 2010.

[17] L. Gauchia, "A per-unit hardware-in-the-loop simulation of a fuel cell/battery hybrid energy system," *IEEE Transactions on Industrial Electronics*, vol. 57, pp. 1186 – 1194, Apr. 2010.

[18] A. Allegre, "Reduced-scale-power hardware-in-the-loop simulation of an innovative subway," *IEEE Transactions on Industrial Electronics*, vol. 57, pp. 1175 – 1185, Apr. 2010.

[19] A. Bouscayrol and J. Irwin, *Control and Mechatronics*. CRC Press, 2011.

[20] V. Pop, H. Bergveld, D. Danilov, P. Peter, and L. Notten, *Battery Management Systems: Accurate State-of-Charge Indication for Battery-Powered Applications*. Springer, 2010.

[21] D. Andrea, *Battery Management Systems for Large Lithium-Ion Battery Packs*. Artech House, Sept. 2010.

[22] K. Etschberger, *Controller Area Network*. IXXAT Automation GmbH, Aug. 2001.

[23] H. Qian, "A high-efficiency grid-tie battery energy storage system," Ph.D. dissertation, Virginia Polytechnic Institute and State University, 2011.

[24] A. Jossen, V. Spath, H. Dring, and J. Garche, "Reliable battery operation - a challenge for the battery management system," *Journal of Power Sources*, vol. 84, p. 283286, Dec. 1999.

[25] G. IEC 60529: Degrees of protection provided by enclosures (IP Code). International Electrotechnical Commission.

[26] H. Kiehne, *Battery Technology Handbook*. John Wiley and Sons, 2003.

[27] D. Linden and T. Reddy, *Handbook of Batteries*. McGraw-Hill, 2002.

[28] D. Doerfel and S. Sharkh, "A critical review of using the peukert equation for determining the remaining capacity of lead-acid and lithium-ion batteries," *Journal of Power Sources*, pp. 395–400, 2006.

[29] K. Ng, C. Moo, Y. Chen, and Y. Hsieh, "Enhanced coulomb counting method for estimating state-of-charge and state-of-health of lithium-ion batteries," *Journal of Applied Energy*, 2008.

[30] J. Stevens and G. Corey, "A study of lead-acid battery efficiency near top-of-charge and the impact on pv system design," *Proc. Photovoltaic Specialists Conference*, May 1996.

[31] E. Sexton, "Coulombic efficiency of a sealed, thin plate, spiral lead-acid battery," *Proc. Battery Conference on Applications and Advances*, pp. 511–520, Jan. 1998.

[32] S. Zoroofi, "Components and packaging technologies, ieee transactions on," Master's thesis, Chalmers University of Technology, 2008.

[33] O. Tremblay, "A generic battery model for the dynamic simulation of hybrid electric vehicles," *Proc. Vehicle Power and Propulsion Conference*, 2007.

[34] P. Mauracher and E. Karden, "Dynamic modeling of lead/acid batteries using impedance spectroscopy for parameter identification," *Journal of Power Sources*, vol. 67, pp. 69–84, July 1997.

[35] S. Buller, M. Thele, D. Doncker, and E. Karden, "Batteries for power electronic applications," *Journal of Industry Applications*, pp. 742–747, 2005.

[36] C. Gould, C. Bingham, D. Stone, and P. Bentley, "New battery model and state-of-health determination through subspace parameter estimation and state-observer techniques," *Journal of Vehicular Technology*, vol. 58, pp. 3905–3916, 2009.

[37] X. Feng and Z. Sun, "A battery model including hysteresis for state-of-charge estimation in ni-mh battery," *Proc. Vehicle Power and Propulsion Conference*, 2008.

[38] B. Y. Liawa, G. Nagasubramanianb, R. Jungstc, and D. Doughtyb, "Modeling of lithium ion cellsa simple equivalent-circuit model approach," *Journal of Solid State Ionics*, 2004.

[39] A. Ramamurthy, "Advanced lithium ion battery modeling and power stage integration technique," *Energy Conversion Congress and Exposition (ECCE)*, pp. 1485 – 1492, 2010.

[40] M. Ceraolo, "New dynamical models of lead-acid batteries," *IEEE Transactions on Power Systems*, pp. 1184 – 1190, Nov. 2000.

[41] S. Chen, "Modeling of lithium-ion battery for energy storage system simulation," *Power and Energy Engineering Conference*, March 2009.

[42] E. davis, D. Funk, and W. Johnson, "Internal ohmic measurement and their relationship to battery capacity-epri's ongoing technology evaluation," *The Battcon 2002 Stationary Battery Conference*, May 2002.

[43] L. Gao, "Dynamic lithium-ion battery model for system simulation," *IEEE Transactions on Components and Packaging Technologies*, sept. 2002.

[44] C. Shepherd, "Design of primary and secondary cells," *Journal of The Electrochemical Society*, no. 112, p. 657, 1965.

[45] O. Tremblay1 and L. Dessaint, "Experimental validation of a battery dynamic model for ev applications," *Journal of World Electric Vehicle*, vol. 3, May 2009.

[46] C. Edrington, "Virtual battery charging station utilizing power-hardware-in-the-loop: Application to v2g impact analysis," *Proc. Vehicle Power and Propulsion Conference (VPPC)*, 2010.

[47] M. Anderson and D. Carr, "Battery energy storage technologies," *Journal of Electric Power Systems Research*, vol. 81, no. 3, Mar. 1993.

[48] W. Lachs, "Application of battery energy storage in power systems," *Proceedings of 1995 International Conference on Power Electronics and Drive Systems*, Feb. 1995.

[49] I. Gyuk, "The united states of storage electric energy storage," *IEEE Power and Energy Magazine*, vol. 3, pp. 31–39, March-April 2005.

[50] X. Wang, D. Vilathgamuwa, and S. Choi, "Determination of battery storage capacity in energy buffer for wind farm," *IEEE Transactions on Energy Conversion*, vol. 23, pp. 868 – 878, Sept. 2008.

[51] N. Mohan, T. Undeland, and W. Robbins, *Power electronics:converters, applications, and design*. John Wiley and Sons, 2003.

[52] T. Brekken, A. Yolochi, A. Jouanne, and H. Hapke, "Optimal energy storage sizing and control for wind power applications," *IEEE Transactions on Sustainable Energy*, vol. 2, pp. 69–77, Jan. 2011.

[53] S. Teleke, M. Baran, A. Huang, S. Bhattacharya, and L. Anderson, "Control strategies for battery energy storage for wind farm dispatching," *IEEE Transactions on Energy Conversion*, vol. 24, pp. 725–732, Sept. 2009.